AMENDMENT TO THE DRAWINGS

A replacement sheet for FIG. 4 is provided under Appendix A. The proposed changes are detailed below in *Section B. Drawing Objections* of this Response. Applicant respectfully requests the Examiner approve the drawings as amended.

REMARKS

A. Status of Claims

Claims 1-9 are pending. Claims 4-5 have been withdrawn. Claims 1-3, 6, 7, and 9 have been amended. Claims 1-3 and 6-9 are presented for reconsideration.

B. Drawing Objections

The drawings stand objected to for allegedly failing to comply with 37 C.F.R. § 1.84(p)(5). Applicant submits a replacement drawing sheet under **Appendix A** correcting the inadvertent error, and in particular, removing reference number 430 from FIG. 4. Applicant submits the changes do not add new matter and respectfully requests the objections to the drawings be withdrawn.

The drawings also stand objected to for allegedly failing to comply with 37 C.F.R. § 1.83(a) because the drawings fail to show every feature of the invention. Applicant respectfully traverses. However, claim 9 has been amended and now recites "The method of claim 8, further comprising creating a photon distribution energy curve of the signal." The element cited in claim 9 is shown, for example, in FIG. 6 and described in the supporting text. Applicant believes that claim 9 and FIG. 6 are in full compliance with 37 C.F.R. § 1.83(a) and respectfully requests the objections to the drawings be withdrawn.

C. Specification Objection

The Specification stands objected under 35 U.S.C. § 112 first paragraph for allegedly failing to provide an adequate written description and for failing to enable one of ordinary skill in the art how to make and use the invention. Applicant respectfully traverses.

1. Components 1 through 5

The Office contends that the Specification fails to provide an adequate description and an enabling description. In particular, the Office contends that the Specification fails to provide the internal components of the PPADs, the scintillator paddles, the converter, the data acquisition and processing system, and the computer program. *See* page 4-5 of the Office Action mailed on 2/13/06. Additionally, the Office states that if the description of the individual components is

described in other references, such references should be provided to the Office. *See* id. Applicant respectfully traverses.

Here, the basis for the written description and enablement rejection is only that no description of the internals of certain components is provided. *See* Office Action, page 4. This fails to rise to a *prima facie* case because no argument or explanation is propounded to address why the Specification is incomplete or why the Specification would not teach one how to make and use the claimed invention without undue experimentation. Instead, it appears that the Examiner expects a longer description than what is given, without any supporting evidence or reasoning, that a longer (or different) description would be required for one to make and use the invention.

If the Office doubts that the Specification shows how to make and use the invention, then it must explain its reasoning. In this regard, Applicant notes that "it is incumbent upon the Patent Office...to explain why it doubts the truth or accuracy of any statement in a supporting disclosure and to back up assertions of its own with acceptable evidence or reasoning which is inconsistent with the contested statement." M.P.E.P. 2164.04 (quoting *In re Marzocchi*, 439 F.2d 220, 224, 169 U.S.P.Q. 367, 370 (CCPA 1971)) (emphasis added). If the Examiner wishes to rely on personal knowledge or evidence in the art to support an enablement rejection, that position would have to be supported by citing published references or by Examiner's Affidavit. M.P.E.P. 2144.03.

Applicant also notes that not everything necessary to practice the invention need be disclosed and what is well-known is best omitted. *In re Buchner*, 929 F.2d 660, 661, 18 USPQ2d 1331, 1332 (Fed. Cir. 1991). All that is necessary is that one skilled in the art be able to practice the claimed invention, given the level of knowledge and skill in the art. Applicant assert that the description of components 1 through 5 in the Specification is full, clear, and concise, and would enable any person with ordinary skill in the art to make and use the components without undue experimentation. For at least these reasons, the objection is improper.

However, in the spirit of cooperation, Applicant provides below example portions of the Specification where each component is fully described. Supporting references or commercial companies with similar components for sale are also provided.

a. A fission-fragment detector or a parallel plate avalanche detector (PPAD) is described in detail, for example, beginning on page 9, line 14 through page 12, line 19 and shown in FIGs. 1 through 4 of the Specification.

Additionally, a Supplemental Information Disclosure Statement (SIDS) is being filed concurrently with this paper. A courtesy copy of the Supplemental Information Disclosure Statement is provided for the convenience of the Examiner under **Appendix F,** and a copy of the reference is provided under **Appendix B**. The reference (co-authored by Applicant) is directed to the design of an example PPAD. Applicant requests that this reference be considered and made of record.

For at least the above reasons, the description provided is complete and adequate.

b. A scintillator paddle is described in detail, for example, in FIG. 1 and beginning on page 7, lines 18 through 22, page 8, line 13 through page 9 line 13. Referring to the reference provided under **Appendix C**, the functionality and different types of scintillator detectors are provided. *See* pages 157-164. Applicant requests that this reference, concurrently submitted in the SIDS, be considered and made of record. Applicant also notes that such detectors may be obtained from, amongst other companies, Saint Gobain Crystals, Newbury, Ohio or from Eljen Technology, Sweetwater, Texas.

For at least the above reasons, the description provided is complete and adequate.

c. A converter is described in detail, for example, in FIG. 1, on page 7, lines 13-18, and on page 9, lines 2-10. The reference provided under **Appendix C** provides how electron pairs are produced. *See* pages 57-59.

For at least the above reasons, the description provided is complete and adequate.

d. A data acquisition system is illustrated in FIG. 5 and described in detail beginning on page 13, line 3 through page 14, line 10.

Referring to the reference provided under **Appendix D**, the functionality of a data acquisition system used in a detector system. *See* pages 351-354. Applicant requests that this reference, concurrently submitted in the SIDS, be considered and made of record.

For at least the above reasons, the description provided is complete and would enable one of ordinary skill in the art to make and use the invention without undue experimentation.

e. A computer program, as defined in the Specification, is

> a sequence of instructions designed for execution on a computer system. A program, or computer program, may include a subroutine, a function, a procedure, an object method, an object implementation, an executable application, an applet, a servlet, a source code, an object code, a shared library/dynamic load library and/or other sequence of instructions designed for execution on a computer system. *See* page 15, lines 10-15.

Applicant asserts that one of ordinary skill in the art, from the definition provided in the Specification, would understand a computer program. For at least the above reasons, the description provided is complete and adequate.

2. Tuning the PPAD

The Office contends that "there is no adequate description or enabling disclosure of how and in what manner different materials are used to tune PPAD 200 to a corresponding range of energies to allow detection of materials in varying atomic numbers." (Office Action, page 5). Applicant respectfully traverses.

The Specification provides, for example, on page 6, lines 9 through 14, that

> In the passage of photons through matter, a photon interacts with atoms or nuclei in an energy-dependent way. Specifically, high atomic number (Z) materials tend to absorb higher energy photons, and low Z materials tend to absorb lower energy photons. The invention includes a method and/or apparatus for measuring the attenuation of a photon beam flux, therefore yielding a measure of the density and distribution of the interrogated material.

To achieve this, the Specification discloses three sets of detectors **135**, **140** and **150** "used to measure the beam of photons **121** emerging from the cargo container **125**." (Page 8, lines 5 through 6). The PPAD **135** may be

> tuned to the photofission cross section of the fissile material to be interrogated in container **125**. In one embodiment, the array of fission-fragment detectors **135** is sensitive to photon energies in the range of about 10 to 20 MeV. In other embodiments, a different range of energies may be desirable.

As noted in the Specification, the "fission-fragment detector **200** may be used as an element of the array of fission-fragment detectors **135** detailed in **FIG. 1**." (Page 10, lines 2 through 4).

Applicant assert that one of ordinary skill in the art, from the description provided in the Specification would understand that the PPADs may be tuned to, *i.e.,* be sensitive to different targets having different responses to the energy of the emerging photon beam, hence "tunable," and thus, would be able to practice the invention without undue experimentation. Applicant respectfully requests the objection to the Specification be withdrawn.

3. Identifying Material

The Office contends that there is no adequate description or enabling disclosure on how and in what matter any material is identified. *See* page 5 of the Office Action. Applicant respectfully traverses.

Referring to FIG. 1 and the supporting text, the Specification provides

> detectors **135**, **140** and **150** can be used to measure the beam of photons **121** emerging from the cargo container **125**. By resolving the energy of the beam **121**, the effective density distribution of the matter within the container **125** may be revealed. Material concealed within the cargo container **125** may selectively absorb the various parts of the bremsstrahlung spectrum of the incident photon beam **120** depending upon its atomic number. The photon flux monitor **130** may register a drop in the emerging photon beam **121** intensity in the energy regime where the interrogated material has preferentially absorbed the photon beam. (Specification, page 8, lines 5-12)

For low-Z materials which interact primarily with the lower energy portion of the emerging photon beam **121**, "the variation of the PMT current may give a measurement of the distribution of low-Z materials within the interrogated vessel **125**. In one embodiment the scintillator paddles **140** are sensitive to photon energies less than about 6 MeV." (Specification, page 8, lines 19-21). Similarly, for high-Z materials, converter foil **145** and scintillator paddles **150** may be used to produce and detect electron/positron pairs, respectively. *See* page 9, lines 1 through 13. In one respect, scintillator paddles **150** are sensitive to photon energies above 6 MeV. *See id.*

The Specification sets forth clearly and concisely how to identify matter by detecting the energy beam (**121**) from the container using, for example, detectors **135**, **140**, and **150**. One of

ordinary skill in the art would recognize how materials are identified given the detailed description provided in the Specification. Applicant respectfully requests the objection to the Specification be withdrawn.

4. Scintillator Paddles

The Office contends that there is no adequate description or enabling disclosure of how and in what manner the scintillator paddles may be a telescopic array. *See* page 5 of the Office Action. Applicant respectfully traverses.

Telescopic array is a term known in the art where the detectors are aligned in a linear fashion. Support for this may be found in the reference under **Appendix E.** *See* FIG. 2 and the supporting text. Applicant requests that this reference, concurrently submitted in the SIDS, be considered and made of record.

For at least the above reasons, the description provided is complete and would enable one of ordinary skill in the art to make and use the invention without undue experimentation.

D. Section § 112, First Paragraph Rejections

Claims 1-3 and 6-9 stand rejected under 35 U.S.C. § 112, first paragraph, as allegedly failing to comply with the written description requirement and enabling requirement, as outlined above with respect to the Specification objection. Applicant respectfully traverses.

Applicant refers the Office to the analysis above, which overcomes these rejections. Applicant respectfully request the removal of the § 112, first paragraph rejections to the claims.

E. Section § 112, Second Paragraph Rejection

Claims 1-3, 6-9 stand rejected under 35 U.S.C. § 112 second paragraph for allegedly failing to particularly point out and distinctly claim the subject matter. Applicant respectfully traverses.

1. Claim 1 is Definite

The Office contends that claim 1 is indefinite for being vague as to where the emerging photon beam originates. *See* page 7 of the Office Action. Claim 1 has been amended and now

recites, in part: "detecting an emerging photon beam from the material." Support for the amendment may be found, for example, in FIG. 1 and the supporting text of the Specification.

The Office also contends that the term "different" and "ranges" are vague, indefinite and incomplete. Applicant traverses.

Independent claim 1 recites, in part: "the first set of scintillator paddles, and the second set of scintillator paddles are sensitive to different ranges of photon beam energy." The Specification clearly sets forth an example of "different" and "range." For example, a first set of scintillator paddles, *e.g.,* scintillator paddles 140 of FIG. 1 "are sensitive to photon energies less than about 6 MeV." (Page 8, line 21). A second set of scintillator paddles, *e.g.,* scintillator paddles 150 of FIG. 1 "are sensitive to photon energies exceeding about 6 MeV." (Page 9, lines 11-12).

Considering this example description of how a first set of scintillator paddles and a second set of scintillator paddles are sensitive to different ranges of photon beam energy of claim 1 in light of the fact that "definiteness of claim language must be analyzed, *not in a vacuum*, but in light of: (A) the content of the particular application disclosure, (B) the teachings of the prior art, and (C) the claim interpretation that would be given by one possessing the ordinary level of skill in the pertinent art at the time the invention was made" M.P.E.P. § 2173.02, 2100-194], Applicant respectfully submits that claim 1 is definite. Applicant respectfully requests the removal of the rejection to claim 1.

Further, the Office states that the limitation does not connote any particular range or indicates if the range overlaps, *etc.* See page 7 of the Office Action. However, based on this claim step, one of ordinary skill in the art would understand that the recited the ranges may vary, and that one or more ranges may be used. Breadth is not indefiniteness. M.P.E.P. § 2173.04.

For at least these reasons, Applicant respectfully submits that claim 1 is definite. Applicant respectfully requests the removal of the rejection to claim 2.

2. Claim 2 is Definite

The Office states that claim 2 is vague, indefinite, and incomplete in what is meant by the term "detecting the material." *See* Office Action, page 8. Claim 2 has been amended and now recites, in part: "determining the atomic number of the material in the container." Support for

the amendment may be found, for example, on page 6, lines 5 through 6. Applicant believes that the amendment clarifies the step of identifying the material. Applicant respectfully requests the removal of the rejection to claim 2.

3. Claim 3, 6, and 7 are Definite

Claims 3, 6, and 7 are allegedly deemed vague, indefinite, and incomplete as the phrase "photon beam energy" by the Office. *See* Office Action, page 9. Applicant traverses. However, claims 3, 6, and 7 have been amended and each now recites detecting an energy from the emerging photon beam. Applicant submits that claims 3, 6, and 7 are definite and respectfully request that the § 112, second paragraph rejection be withdrawn.

4. Claim 9 is Definite

Claim 9 stands rejected for improper antecedent basis. Applicant has amended the inadvertent error. Support for the amendment may be found, for example, on page 14, lines 8-10. Applicant respectfully requests the removal of the rejection to claim 9.

5. Claim 3 is Definite

Claim 3 stands rejected for are allegedly being vague, indefinite, and incomplete based on the element "about 10 to 20 MeV." *See id.* In particular, the Office rejects the element "10" for lack of units and for the term "about." *See id.* Claim 3 has been amended to recite "10 MeV."

Applicant submits that the term "about" is definite. *See* M.P.E.P § 2173.05(b) (claim language including terms of degree does not automatically render the claim indefinite). The term "about" has been deemed definite if it can clearly be assessed. Here, one of ordinary skill in the art would know what is meant by the use of "about 10 MeV to 20 MeV) in claim 3.

For at least the above reasons, claim 3 is definite. Applicant respectfully requests the removal of the rejection to claim 3.

6. Claims 1-3 and 6-9

Claims 1-3 and 6-9 stand rejected under 35 U.S.C. § 112, second paragraph for allegedly omitting essential steps. Applicant respectfully traverses.

Applicant notes that the second paragraph of 35 U.S.C. § 112 is directed to the requirements that the claims particularly point out and distinctly claim the subject matter which the Applicant regards as his invention. The claims, however, are not required to recite each and every step that could be performed during use of the method or to recite specifically how each step of the method could be performed. For example, the claims particularly point out and distinctly claim the subject matter that Applicant regards as his invention even though the claims do not recite additional specific steps that can be employed. If the scope of the subject matter is clear, and if Applicant have not otherwise indicated that they intend the invention to be of a scope different from that defined in the claims, then the claims comply with 35 U.S.C. 112, second paragraph. M.P.E.P. § 2173.04.

However, claim 1 has been amended and now recites a step for identifying the material. Support for the amendment may be found, for example, on page 6, lines 4-6, which states a method for "measuring fluxes of transmitted photons in the regime of high energies, thereby determining the atomic number of the material on the photon beam path."

For at least these reasons, claim 1 and its dependent claims are complete. Removal of the § 112 rejection is requested.

F. Section 102 Rejections

Claims 1-3 and 6-9 stand rejected under 35 U.S.C. § 102(b) as allegedly being anticipated by the reference entitled "Associated Particle Sealed Tube Neutron Probe for Characterization of Materials" by Rhodes *et al.* In light of the above claim amendments and below comments, Applicant respectfully traverses.

Claim 1 has been amended and now recites:

casting an incident photon beam on the material;

detecting an emerging photon beam from the material with an array of fission-fragment detectors, a first set of scintillator paddles, and a second set of scintillator paddles, wherein the array of fission-fragment detectors, the first set of scintillator paddles, and the second set of scintillator paddles are sensitive to different ranges of photon beam energy; and

determining a photon energy regime of the emerging photon beam, the photon energy level identifying the material.

Support for the amendment may be found, for example, in FIG. 6 and the corresponding text. The Specification discloses that in "passage of photons through matter, a photon interacts with atoms or nuclei in an energy-dependent way. Specifically, high atomic number (Z) materials absorb higher energy photons, and low Z materials tend to absorb lower energy photons." (Page 6, lines 9-11). The element of determining a photon energy level of the emerging photon beam, the photon energy level identifying the material, amongst others, is absent in the Rhodes publication.

The Rhodes publication is directed to neutron diagnostic probe system. *See* Abstract. In one respect, to detect contraband, a fast-neutron transmission imaging (FNTI) system and a gamma-ray transmission imaging (GRTI) are used. *See* Section 4.2. Neither of these systems determines a photon energy level of the emerging photon beam, the photon energy level identifying the material, as recited in claim 1. Rather, the FNTI detects spatial attenuation and the GRTI detects gammy-rays. *See id.*

Additionally, the Rhodes reference fails to teach or suggest detecting an emerging photon beam from the material with an array of fission-fragment detectors, a first set of scintillator paddles, and a second set of scintillator paddles, wherein the array of fission-fragment detectors, the first set of scintillator paddles, and the second set of scintillator paddles are sensitive to different ranges of photon beam energy. Neither the FNTI system and/or the GRTI system include an array of fission-fragment detectors, a first set of scintillator paddles, and a second set of scintillator paddles. *See id; see also* FIG. 15.

For at least the above reasons, claims 1 and dependent claim 2 are patentably distinct over the Rhodes publication. Applicant respectfully requests the removal of the § 102 rejection to claim 1 and its dependent claims.

G. Section 103 Rejections

Claims 1-3 and 6-9 stand rejected under 35 U.S.C. § 103(a) as allegedly being obvious over U.S. Patent No. 6,195,413 to Geus *et al.* or U.S. Patent No. 5,742,660 to Majewski *et al.* In light of the above claim amendments and below comments, Applicant respectfully traverses.

1. The Combination of the Geus and Rhodes References Does Not Render the Claims Obvious

As noted above, the Rhodes reference fails to teach or suggest detecting an emerging photon beam from the material with an array of fission-fragment detectors, a first set of scintillator paddles, and a second set of scintillator paddles, wherein the array of fission-fragment detectors, the first set of scintillator paddles, and the second set of scintillator paddles are sensitive to different ranges of photon beam energy or determining a photon energy level of the emerging photon beam, the photon energy level identifying the material. The Geus reference does not provide the deficiencies.

The Geus reference is directed to detecting x-rays. *See* Abstract. To achieve this, Geus provides generating two separate signals FX_L and FX_H from the material and transmits these signals to an image evaluation unit 12 where the "materials in object 2 are evaluated and identified." (Column 5, lines 17-20). Like the Rhodes reference, the Geus reference fails to identify determining a photon energy level of the emerging photon beam, the photon energy level identifying the material, as recited in claim 1. Rather, Geus determines the material based on image construction.

Further, the Geus reference also fails to teach detecting an emerging photon beam from the material with an array of fission-fragment detectors, a first set of scintillator paddles, and a second set of scintillator paddles, wherein the array of fission-fragment detectors, the first set of scintillator paddles, and the second set of scintillator paddles are sensitive to different ranges of photon beam energy, as recited in claim 1. Nowhere in the Geus reference is an array of fission-fragment detectors and a first set and second set of scintillator paddles taught or suggested.

For at least the above reasons, claims 1 and dependent claim 2 are patentably distinct over the combination of the Geus reference and Rhodes reference. Applicant respectfully requests the removal of the § 102 rejection to claim 1 and its dependent claims.

2. The Combination of the Majewski and Rhodes References Does Not Render the Claims Obvious

The Majewski reference is directed to obtaining an x-ray image using a raster scanning technique over an object. *See* Summary of the Invention. In one respect, using a point detector 24, an ytrrium aluminum perovskite (YAP), or a single dual sensitive detector, focused x-rays

contribute to the image produced. *See* column 4, lines 18-24 and lines 55-58; *see also* column 5,lines 35-39; *see also* FIGs. 2, 3, and 5. Nowhere in the Majewski reference is detecting an emerging photon beam from the material with an array of fission-fragment detectors, a first set of scintillator paddles, and a second set of scintillator paddles, wherein the array of fission-fragment detectors, the first set of scintillator paddles, and the second set of scintillator paddles are sensitive to different ranges of photon beam energy taught or suggested.

Furthermore, Majewski fails to teach or suggest determining a photon energy level of the emerging photon beam, the photon energy level identifying the material.

For at least the above reasons, neither the Majewski reference nor the Rhodes reference, separately or combined, teaches or suggests the elements of claim 1. Therefore, claim 1 and its dependent claims are patentably distinct over the cited references. Applicant respectfully requests the removal of the § 103 rejection.

3. The Combination of the Bruschini Reference with the Geus or Majewski References Does Not Render the Claims Obvious

Claims 1-3 and 6-9 stand rejected under 35 U.S.C § 103(a) as allegedly being obvious over the publication entitled "Commercial Systems for Direct Detection of Explosives" by Bruschini in view of the Geus reference or Majewski reference. Applicant respectfully traverses.

As noted above, neither the Geus reference nor Majewski reference teaches or suggests detecting an emerging photon beam from the material with an array of fission-fragment detectors, a first set of scintillator paddles, and a second set of scintillator paddles, wherein the array of fission-fragment detectors, the first set of scintillator paddles, and the second set of scintillator paddles are sensitive to different ranges of photon beam. The Bruschini reference fails to provide the deficiencies.

The Bruschini reference is directed to characterizing existing technologies for use of direct detection of explosives. *See* page 3, section entitled "Introduction." In one respect, the Bruschini reference disclose x-ray based systems such as backscatter systems (measuring backscatter from the object), dual energy x-ray systems (adding color to an image and discriminating the image based on power), computed tomography systems (generating cross-sectional slices of the object and reconstructing the slices to produce a 3D image) for determining an object. None of these systems teach or suggest detecting an emerging photon

beam from the material with an array of fission-fragment detectors, a first set of scintillator paddles, and a second set of scintillator paddles, wherein the array of fission-fragment detectors, the first set of scintillator paddles, and the second set of scintillator paddles are sensitive to different ranges of photon beam.

The Bruschini reference also discloses gamma spectroscopy neutron based technology and system for detecting explosives. *See* section entitled "Gamma Spectroscopy Neutron Based Techniques." This systems generally include gamma detectors such as a counting device, high purity germanium detectors, bismuth germanate detectors, or sodium iodide scintillator. However, these detectors cannot be construed as an array of fission-fragment detectors, a first set of scintillator paddles, and a second set of scintillator paddles, as recited in claim 1.

For at least the above reasons, claim 1 and its dependent claims are patentably distinct over the cited references. Applicant respectfully requests the removal of the § 103 rejections to claims 1-3 and 6-9.

4. Hindsight is Impermissible

The Office contends that it would have been obvious to one of ordinary skill in the art at the time of the invention, detectors sensitive to different energy levels would have been obvious. *See* Office Action page 10 (with respect to the Rhodes reference); *see also* page 11 (with respect to the Bruschini reference). In deriving its contentions, the Office is evidently proceeding with an impermissible hindsight analysis of the invention. To imbue one of ordinary skill in the art with knowledge of the instant invention, where no prior art reference or references of record convey or suggest that knowledge, is to fall victim to the insidious effect of a hindsight syndrome wherein that which only the inventor taught is used against its teacher. *W.L. Gore Assoc., Inc. v. Garlock, Inc.*, 220 USPQ 303, 312-313 (Fed. Cir. 1983).

Applicant submits that the Bruschini reference and the Rhodes reference fail to anticipate or make obvious claim 1. For at least these reasons, independent claim 1 and its dependent claims are patentably distinct over the cited references. Applicant respectfully requests the removal of the § 103 rejection.

CONCLUSION

Applicant believes that the foregoing remarks fully respond to all outstanding matters for this application. Applicant respectfully requests that the rejections of all claims be withdrawn so the claims may swiftly pass to issuance.

Should the Office desire to sustain any of the rejections discussed in relation to this Response, the courtesy of a telephonic conference between the Examiner, the Examiner's supervisor, and the undersigned attorney at 512-536-3018 is respectfully requested in advance.

Respectfully submitted,

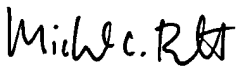

Michael C. Barrett
Reg. No. 44,523
Attorney for Applicant

FULBRIGHT & JAWORSKI, L.L.P.
2400 One American Center
600 Congress Avenue
Austin, TX 78701
Telephone: 512/536-3018
Facsimile: 512/536-4598

Date: June 6, 2006

ELSEVIER Nuclear Instruments and Methods in Physics Research A 441 (2000) 525–534

NUCLEAR INSTRUMENTS & METHODS IN PHYSICS RESEARCH Section A

www.elsevier.nl/locate/nima

Parallel-plate avalanche detectors with anode wire grids

J.C. Sanabria[a,1], B.L. Berman[a,*], C. Cetina[a], P.L. Cole[a,2], W.R. Dodge[a,3], V.G. Nedorezov[b], A.S. Sudov[b], G.Ya. Kezerashvili[c]

[a]*Center for Nuclear Studies, Department of Physics, The George Washington University, Washington, DC 20052, USA*
[b]*Institute for Nuclear Research, Russian Academy of Sciences, Moscow 117312, Russia*
[c]*Budker Institute of Nuclear Physics, Novosibirsk 630090, Russia*

Received 4 June 1999; accepted 31 July 1999

Abstract

A fission-fragment detection system was designed and built at The George Washington University, to be used in photofission experiments at the Saskatchewan Accelerator Laboratory and the Jefferson Laboratory. The fission fragments were detected using parallel-plate avalanche detectors with anode wire grids. An array of several target–detector pairs was mounted inside a low-pressure reaction chamber. The results of calibrations of the detectors using a ^{252}Cf source and their performance with a bremsstrahlung photon beam during the experiments are presented.

Keywords: Parallel-plate avalanche detectors; Fission-fragment detection

1. Introduction

A fission-fragment detection system was designed and built at The George Washington University in order to measure the absolute photofission cross sections for the actinides ^{237}Np, ^{238}U, ^{235}U, ^{233}U, and ^{232}Th and for the preactinides ^{197}Au and ^{NAT}Pb with 3% statistical precision and less than 5% systematic uncertainty. The measurements were performed at the Experimental Area 2 of the Saskatchewan Accelerator Laboratory (SAL), and at the Experimental Hall B of the Jefferson Laboratory (JLab), covering the energy range from 60 MeV up to 4 GeV. The targets of the aforementioned isotopes were irradiated with tagged real photons from a bremsstrahlung beam, and for each photofission event one of the two resulting fission fragments was detected.

Fig. 1 shows the conceptual setup for these experiments. An electron beam incident on a thin radiator generates a bremsstrahlung photon beam in the forward direction. After the radiator, the electron beam is deflected away from the beam line by a dipole magnet, and the energy of each individual electron is measured by an array of

* Corresponding author. Tel.: + 1-202-994-6275.
E-mail address: berman@gwu.edu (B.L. Berman)
[1] Present address. Departamento de Física, Universidad de los Andes, A.A. 4976, Bogotá, Colombia.
[2] Present address. Department of Physics, University of Texas, El Paso, TX 79968, USA.
[3] Retired.

0168-9002/00/$ - see front matter
PII: S0168-9002(99)00857-8

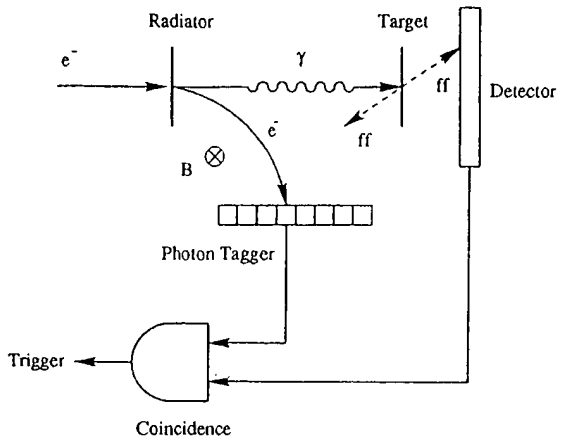

Fig. 1. Photofission experiment with a photon tagger.

scintillators located in the focal plane of the deflecting magnet (photon tagger). The photons continue downstream and traverse a target foil. When a photofission event occurs, two fission fragments are emitted in opposite directions (the linear momentum transferred by a photon to a heavy nucleus is negligible in this energy range; therefore, the center-of-mass and laboratory frames are nearly the same). If one of the emitted fission fragments goes through the fission-fragment detector, the event is registered. The energy of the photon is determined from the difference in energy of the incident electron beam and the electron detected in the focal plane of the tagger. The electronic coincidence between the signals coming from the fission-fragment detector and one of the photon-tagger channels determines the experimental trigger.

As long as the target foils and the fission-fragment detectors are nearly transparent to the photon beam, one can place several target–detector pairs along the beam line, in order to measure simultaneously the photofission cross sections for different isotopes and to increase the statistics of the experiment by using several targets per isotope.

Another way to increase the counting rate is by tilting the target–detector pairs with respect to the beam line. In this way, the amount of target material along the photon beam line is increased with no effect on the detection efficiency (the fission fragments are emitted isotropically in the laboratory frame). As will be explained later, the need for collimation of the fission fragments due to the α activity of the actinide targets used in these experiments did not allow them to be tilted.

Because of the significant difference in photofission cross sections between actinide and preactinide nuclei, the experimental set-up for each set of isotopes was different. The actinide cross sections were measured by having three targets per isotope. The much smaller preactinide cross sections were measured by having several targets of this kind, all tilted by 45° with respect to the photon beam line.

2. Fission-fragment detector system

The detectors of choice were parallel-plate avalanche detectors (PPADs) because they are known to be very efficient in detecting fission fragments [1–8]. They are also ideal for photofission experiments because they have good time resolution (allowing the use of the photon-tagging technique), and they are practically insensitive to neutrons, photons, and electrons. And although PPADs are sensitive to α particles, which are a common source of background when the targets are actinide nuclei, they provide good pulse-height discrimination between the α particles and the fission fragments.

PPADs were also ideal for these experiments because they can be quite transparent to a high-energy photon beam, allowing the use of a sizable array of target–detector pairs along the beam line. This is very important in order to increase the statistics of the measurements, a common problem for photofission experiments, especially for the case of preactinide nuclei. It should also be pointed out that PPADs have a low production cost, as compared for example with solid-state detectors, allowing us to build many of them (50 in this case).

One of the problems when detecting fission fragments with PPADs is that before the fragments enter the active region of the detector, they have to go through one of the electrode planes, usually in the form of a film of conductive material. The energy losses of fission fragments in matter can be very large, and therefore the electrode-film must be very thin. This could represent a serious technical problem in the construction and operation of

the detectors. One of the typical solutions to this problem is to have the target foil serve as one of the electrodes. In the case of actinide nuclei, the radioactive nature of these isotopes makes this solution somewhat risky (obviously, this is not possible when the target is not a conductor), and cannot be used if the foil oxidizes (like Th). The alternative we chose is to replace one of the electrodes by a wire grid, so that most of the fission fragments enter the active region of the detector without interacting with the electrode material. For these experiments, PPADs with anode wire grids were designed, built, and tested at The George Washington University Nuclear Detector Laboratory.

3. Avalanche detectors

PPADs are ionization detectors that operate in the avalanche regime, which is defined by a combination of gas pressure and electric field such that a single free electron can start an exponential ionization process [9]. The pressure required is roughly between a few mTorr and about 25 Torr. The corresponding electric field varies from about 100 to 400 V/mm.

A PPAD is a two-parallel-plate capacitor filled with gas at low pressure, and a voltage applied between the plates, so that the conditions for an avalanche regime are generated across the gap. When a free electron is created inside the detector by an ionizing particle, it will generate an avalanche of electron–ion pairs [10–12]. The number of avalanche electrons is proportional to the distance that they travel,

$$dn_e = n_e \alpha \, dy \tag{1}$$

where n_e is the number of electrons generated between y and $y + dy$, and α is the first Townsend coefficient. This coefficient represents the mean number of ionizing collisions per mm by one electron, and has a very strong dependence on the ratio E/p, where E is the electric field and p is the pressure. From Ref. [1], the voltage pulse generated by a particle track is equal to

$$V = m \frac{e}{C} \frac{\exp(\alpha d)}{(\alpha d)^2} \tag{2}$$

where e is the electron charge, C is the detector capacitance, d is the distance between electrodes, and m is the total number of primary electrons generated by the ion inside the gap.

One of the problems of PPAD design is the high probability of electric breakdown in the form of sparks and glow discharges in the avalanche regime. To minimize this problem, a gas with high self-quenching properties has to be used. Hydrocarbons are the usual choice. Isobutane has been shown to be a good option because it is very common, easy to handle, inexpensive, and provides a satisfactory response [2].

4. PPAD design

In our design the anode plane of the PPAD is a grid of gold-plated tungsten/rhenium wires, and the cathode plane is an aluminized mylar foil. The frames for both electrodes are rectangles of PC-Board material (FR-4, which is a kind of fiberglass), with windows cut inside. The thickness of each FR-4 frame is 1.5 mm. They are placed back to back, generating a gap between the electrodes of 3 mm. Part of the copper on the external side of the PC boards is removed to provide the necessary space for connecting resistors, capacitors, HV connectors, and signal connectors. It is also important to remove copper from the edges of the windows to minimize the probability of electric breakdown along the limits of the active region. To minimize this probability even further, the cathode windows are made 10 mm × 10 mm larger in area than the anode windows; in this way the profile of the edge of the window is not a straight line, and the distance along that surface traveled by the breakdown electrons is maximized. The edges of the windows are also rounded to prevent electric discharges from developing near sharp edges. Fig. 2 shows the basic design and some relevant dimensions.

The grid wires are attached to the anode frame with epoxy glue, and electrically connected to the copper area of the PC board with conductive epoxy glue. The wires are 25 μm in diameter and are spaced 1 mm from each other. The aluminized Mylar foil for the cathode also was glued with

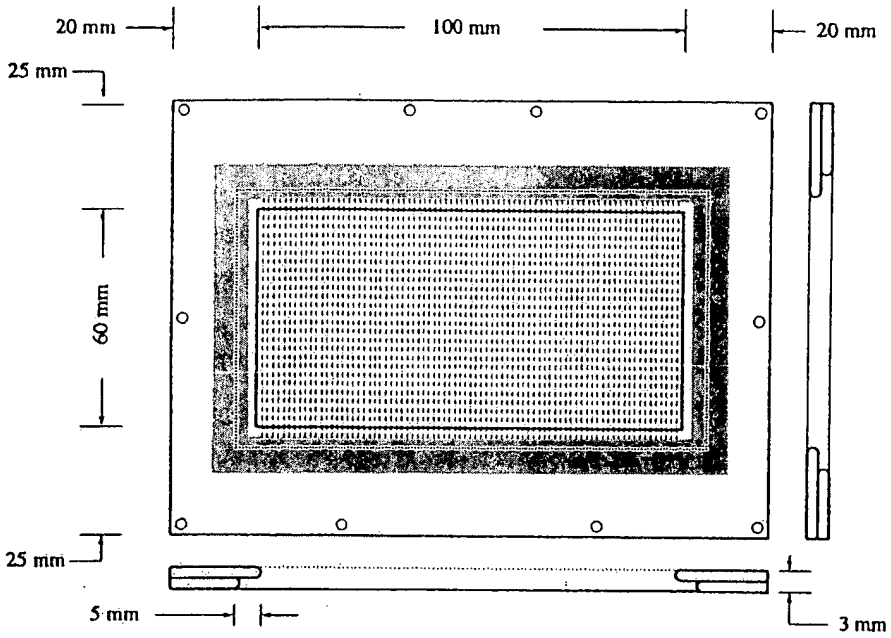

Fig. 2. PPAD design.

conductive epoxy to the frame, and is secured with non-conductive epoxy glue. After testing the first prototypes using a transparent reaction chamber (made out of plexiglass), it was concluded that any metallic area exposed to the low-pressure isobutane atmosphere is a potential source of electric breakdown. To prevent this from happening, all the exposed areas are covered with a layer of epoxy glue, and the high voltage connectors are encapsulated in plastic cases.

In Fig. 3 the electric circuit for a PPAD is shown. The function of this circuit is to provide a match with the 50-Ω input impedance of the analog amplifier, and a low-pass filter for any noise coming from the high-voltage power supply. To reduce the noise level even further, the signals are fed out using coaxial cables and connectors (LEMO connectors).

A target foil was placed in front of each PPAD. The targets were aluminum foils nominally 100 μm thick, with a film of fissionable material deposited on one side. Each target was sandwiched between two FR-4 frames with 5 mm × 10 mm windows. They were connected to the detectors by long Teflon screws, and the distance between the targets and the detectors was set by Teflon spacers.

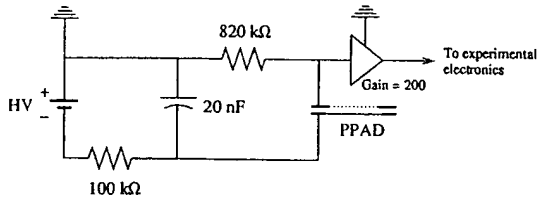

Fig. 3. PPAD circuit diagram.

The PPADs were designed with a rectangular shape in order to allow them to be tilted 45° with respect to the beam line if necessary. Although by doing this the counting rate of the experiment can be increased, the energy resolution is decreased. Particles that enter the active region at large angles will produce larger signals than those that enter at smaller angles. As a result, the α-particle and the fission-fragment spectra will have longer tails and thus will tend to overlap. Since the actinide nuclei are α active, this overlap can compromise the particle discrimination. After prototype testing, it was concluded that for the actinide targets it was necessary to constrain the angles of the particles coming into the detector by placing a collimator in front of

the anode. The collimators were FR-4 sheets, 1 mm thick, with a circular hole (40 mm in diameter) in the center. Similar collimators were placed next to the targets, in order to limit the number of α particles emitted by the targets and reaching the detectors.

In the case of the actinide targets, the distance to the detectors was 17.5 mm and two collimators were used. In the case of the preactinide targets, since they are not α active, there was no need for collimation. The targets were also put as close as possible to the detectors to maximize the solid-angle acceptance, and the pairs were tilted 45° with respect to the beam line. Fig. 4 shows the different parts of a typical target–detector pair.

In order to provide the low-pressure isobutane atmosphere necessary for the operation of the PPADs, the array of target–detector pairs was placed inside a hermetically sealed reaction chamber built at the Kurchatov Institute in Moscow. The chamber is a box with a 120 cm × 20 cm × 16 cm inner volume. The body of the chamber is made out of steel with the exception of the lid that is made out of aluminum (so that it can be removed more easily). The target–detector pairs were suspended from the inner side of the lid, connected to it by two rails. Once the lid of the chamber was in place, the center point of the targets and detectors were aligned with the center point of the two thin windows at the ends of the chamber. The windows were fabricated by milling out a cylindrical portion from an aluminum flange, until only a thin layer (0.5 mm thick) was left. The two center points of the windows were aligned with the photon beam line, ensuring that the beam would go through the center of all the targets and detectors. Fig. 5 shows the reaction chamber and the array of target–detector pairs inside.

The high voltage is delivered to the detectors inside the chamber via a 20-channel feedthrough. To extract the detector signals, three 10-channel signal feedthroughs were used. All the feedthroughs are installed in flanges mounted at the ends of the lid; in this way all the detectors and their electric connections can be removed from the chamber by removing its lid. The maximum number of target–detector pairs that can comfortably be installed inside the chamber is 24.

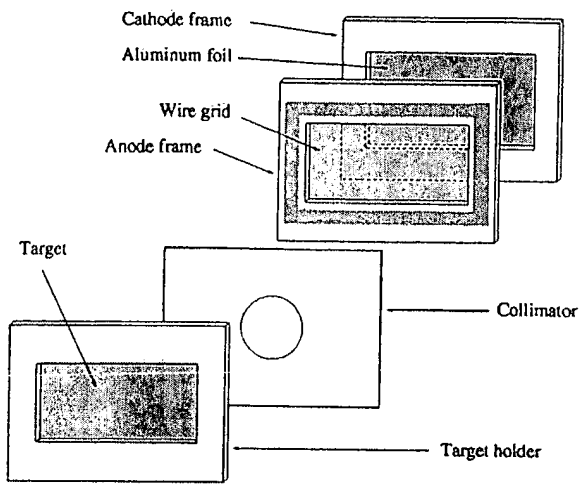

Fig. 4. Target–detector pair.

To maintain the avalanche regime, and to keep the gain of avalanche detectors constant, it is necessary to keep the pressure and purity of the gas stable. One of the options to achieve this is to flow the isobutane through the chamber using an accurate pressure and flow control system. Since the time resolution of the photon taggers at SAL and JLab is of the order of 2 ns, it was concluded that, as long as the gas was exchanged every 24 h, the time resolution of the PPADs would be good enough to match that of the photon tagger. Therefore, we were able to simplify the gas control system greatly. A schematic diagram is shown in Fig. 6. To monitor the pressure of the gas, a species-independent pressure gauge was installed. The pressure gauge was connected to the data-acquisition system through an analog-to-digital converter, and the value of the pressure was recorded every 10 seconds. As for the purity of the gas, a PPAD and a ^{252}Cf source were installed inside the chamber, but out of the beam line. By monitoring the change in the ADC spectrum for the spontaneous-fission fragments from ^{252}Cf, changes in the gain of the other detectors could be inferred, and these changes could be associated with the degradation of the gas quality.

The reaction chamber was mounted on a movable table, screw-driven by a stepping motor, so that it could be removed from the photon beam

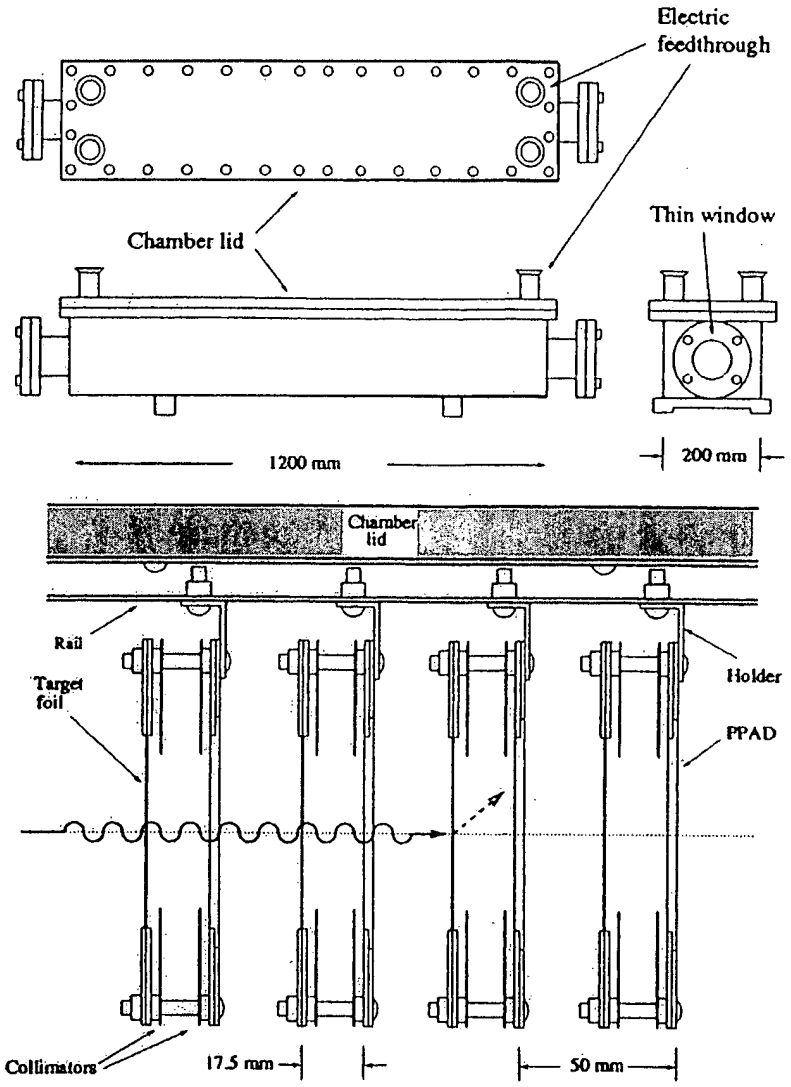

Fig. 5. Reaction chamber and target–detector array.

line remotely. This was necessary when performing tagging-efficiency runs and other tests to measure background levels. The table was designed and built by the technical staff of SAL.

5. Detector testing

When prototyping a PPAD, one of the advantages is that one can use spontaneous-fission sources to test the detector. The properties of the fission fragments emitted by a source like ^{252}Cf are almost identical to those of the fragments emitted by induced fission.

During the prototyping and production of the 50 PPADs built at The George Washington University Nuclear Detector Laboratory, two ^{252}Cf sources were used. One was a thick source (the californium was deposited on top of a metallic disk), and the other one was thin (the californium

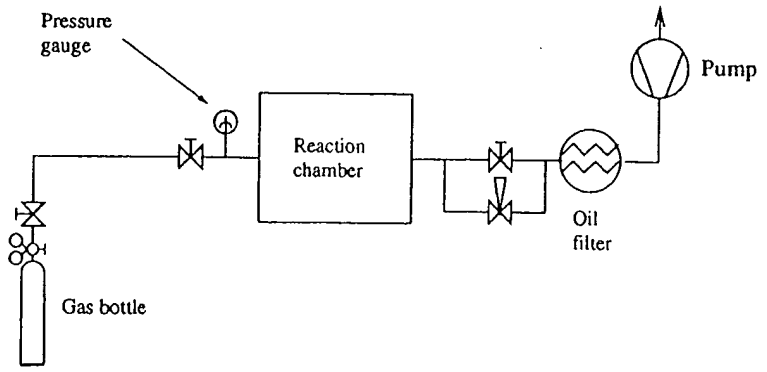

Fig. 6. Reaction-chamber gas system.

was deposited on a very thin film of aluminum oxide). With the thick film, the energy spectrum recorded by a PPAD was studied. The dependence of this spectrum on the size of the collimator, the distance between the target and the detector, and the pressure and the purity of the gas was characterized. In Fig. 7 the ADC spectrum for ^{252}Cf is shown.[4] The very good separation between the α particles (the low-energy tail) and the fission fragments is due mostly to the narrow collimation of the fragments. Because of the beam spot size, especially at SAL, and the need for a high counting rate during the experiment, such narrow collimation was not possible. In spite of this, reasonably good discrimination between α particles and fission fragments was achieved.

The thin californium film allows both of the fragments emitted during a spontaneous fission to escape. By placing one PPAD on one side of the film and another one on the other side, the time difference between the signals coming from both PPADs yields information about the combined time resolution of both detectors. Several tests of this kind were performed, and the time resolution for the PPADs was evaluated. These tests showed that the time resolution for the PPADs is very sensitive to the geometrical configuration of the two detectors, the quality of the gas, the gas pressure, and the applied voltage. However, the main conclusion of all these studies was that the time

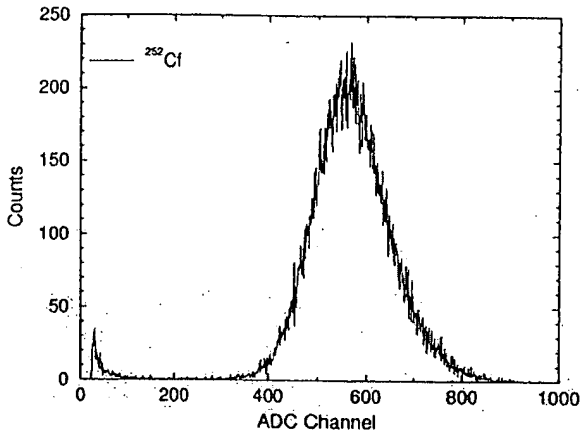

Fig. 7. ADC spectrum for a PPAD test with a ^{252}Cf source. Pressure = 10 Torr, V = 650 V, collimator diameter = 10 mm.

resolution for this design is at most 1 ns, which was good enough for the purposes of the photofission experiments.

The average peak voltage of the pulses generated by fission fragments on a PPAD was of the order of 5 mV, while for α particles it was of the order of 1 mV. By using a fast linear amplifier with a gain of 200, the fission-fragment signals were amplified to about 1 V, which is within the range of voltages accepted by standard instrumentation modules. The signal risetime was 6 ns, and the decay time was 12 ns.

To test each of the PPADs produced, and also to characterize their dependence on electric field and gas pressure, measurements of the counting rate of

[4] For this test, a LeCroy 2249A ADC was used.

^{252}Cf fragments at different voltages and gas pressures were performed. Fig. 8 shows the results of some of those tests. From this figure we can see that as the pressure of the isobutane decreases, the counting rate as a function of applied voltage becomes a smoother curve. However, the probability of destructive electric breakdown also becomes a significant problem. For this reason it was decided that a safe operating point was with a pressure of 15 Torr and a voltage of about 750 V.

6. Detector efficiency

A PPAD is a very efficient fission-fragment detector. Most of the inefficiency comes from the interception of fission fragments by the wire grid that forms the anode plane. In the case of the actinide targets, the collimators limit the angles at which the particles enter the active region; therefore, the inefficiency is approximately equal to the fraction of area covered by the wires, which is 2%, resulting in a detection efficiency of 0.98.

In the case of the preactinide targets, some particles can enter the active region at very wide angles, and the density of wires that could obstruct the particle's path increases significantly. To account for this effect, a geometrical calculation of the effective area covered by the wires for a large solid angle, as "seen" by a fission fragment, was made. The detection efficiency calculated in this manner was determined to be 0.96.

7. Detector performance

During the experiments at SAL and JLab, energy and timing information was read out for each photon-induced fission event. The energy content of each signal produced by a PPAD was measured by an ADC. To determine the number of fission events induced by tagged photons, the basic information came from the TDC spectrum of each tagger channel. The TDC was started by a signal coming from a PPAD and it was stopped by a signal in the tagger channel. The event was accepted and read out by the DAQ system if the two signals were within a given resolving time.

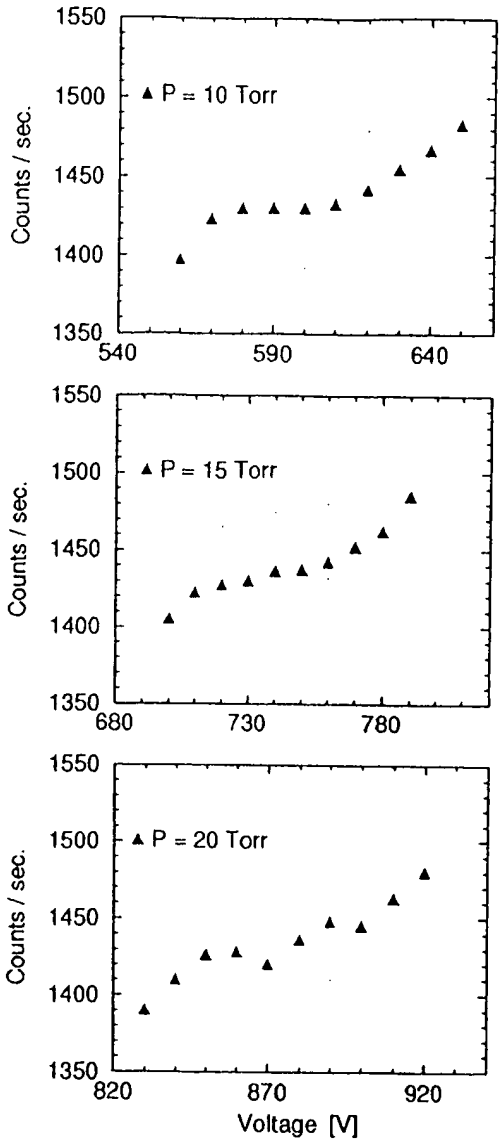

Fig. 8. Counting rate as a function of voltage and pressure for a ^{252}Cf test of a typical PPAD.

In many cases the signal in the PPAD is produced either by a fission event induced by an untagged photon or by an α particle. For such events, the fact that the PPAD signal might be in coincidence with the signal from a tagger channel is an accident. However, there is no time correlation between those two signals, and these kinds of

events (accidental coincidences) therefore produce a flat background in the TDC spectrum.

When the PPAD signal is the result of a fission event induced by a tagged photon, there is a time correlation between this signal and the signal produced in one of the tagger channels by the corresponding electron. These kinds of events (true coincidences) appear in the TDC spectrum as a narrow peak with a width of about 2.5 ns, which is the combined resolution time of the PPADs and tagger channels. Therefore, the inferred time resolution for an individual PPAD can be estimated to be of the order of less than 1 ns (at a pressure of 15 Torr). Fig. 9 shows the TDC spectrum for one of the ^{237}Np targets. In this example the contributions of several tagger channels have been combined to enhance the statistics.

In Fig. 10 a typical ADC spectrum is presented. The decaying distribution in the low energy part is the contribution of the α particles; the other distribution comes from fission fragments (tagged and untagged). The two distributions overlap due to the wide collimation used during the experiments. In spite of the overlap, one can still discriminate the events whose ADC channel number is low enough so that it cannot be the result of a fission fragment. For example, for the case of Fig. 10, events whose ADC channel number is below ~ 75 can be excluded. In this way most of the α particles were easily eliminated from the data.

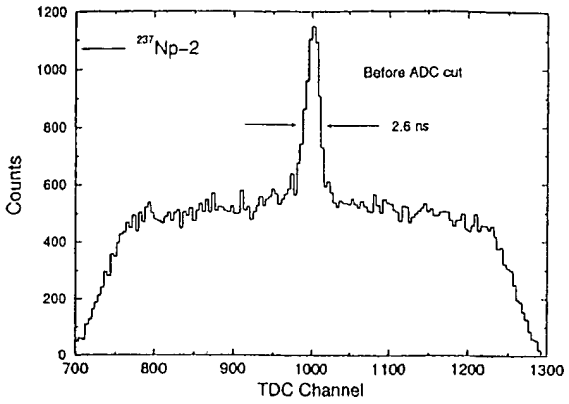

Fig. 9. Tagger TDC spectrum for the target ^{237}Np-2 before ADC cut.

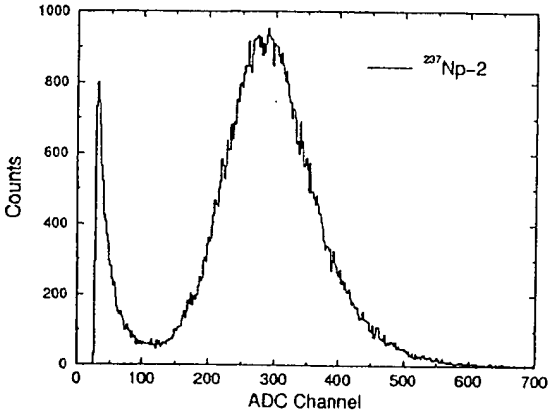

Fig. 10. ADC spectrum for the target ^{237}Np-2.

8. Conclusions

A fission-fragment detection system consisting of a low-pressure reaction chamber and a set of parallel-plate avalanche detectors has been designed and built at The George Washington University. The detection system has been used in two experiments on photofission of actinide and preactinide nuclei at SAL and JLab. The detectors have demonstrated very good stability and reliability under intense bremsstrahlung beams during more than 60 d of data taking. The observed time resolution is of the order of 1 ns when operated at a gas pressure of 15 Torr. The energy resolution of the detector was high enough to allow for very good discrimination between α particles and fission fragments. Finally, due to the simplicity of the design, the aforementioned goals have been achieved at very low cost.

Acknowledgements

The authors are grateful to Professor Gerald Feldman from The George Washington University, and Professor Robert E. Pywell from the University of Saskatchewan for their support and advice during the design and construction of the detectors, and to Professor Reinhard Schumacher and Mr. Gary Wilkin from Carnegie Mellon University for allowing us to use their machine shop and providing us with the technical support.

Work supported in part by the US Department of Energy under Grant No. DE-FG02-95ER40901.

References

[1] G. Hempel, F. Hopkins, G. Schatz, Nucl. Instr. and Meth. 131 (1975) 445.
[2] H. Stelzer, Nucl. Instr. and Meth. 133 (1976) 409.
[3] G. Gaukler et al., Nucl. Instr. and Meth. 141 (1977) 115.
[4] A. Breskin, N. Zwang, Nucl. Instr. and Meth. 144 (1977) 609.
[5] Y. Eyal, H. Stelzer, Nucl. Instr. and Meth. 155 (1978) 157.
[6] M. Just et al., Nucl. Instr. and Meth. 148 (1978) 283.
[7] W. Gunter et al., Nucl. Instr. and Meth. 163 (1979) 459.
[8] J.D.T. Arruda-Neto et al., Nucl. Instr. and Meth. 190 (1981) 203.
[9] H. Raether, Electron Avalanches and Breakdown in Gases, Butterworths, London, 1964.
[10] R.W. Pidd, L. Madansky, Phys. Rev. C 75 (1949) 1175.
[11] F.W. Busser et al., Z. Physik 187 (1965) 243.
[12] J. Christiansen, Z. Phys. 4 (1952) 326.

William R. Leo

Techniques for Nuclear and Particle Physics Experiments

A How-to Approach

Second Revised Edition
With 256 Figures, 40 Tables and Numerous Worked Examples

Springer-Verlag
Berlin Heidelberg New York
London Paris Tokyo
Hong Kong Barcelona
Budapest

Dr. William R. Leo

Route de St. Maurice 34, CH-1814 La Tour de Peilz
Switzerland

ISBN 3-540-57280-5 2. Auflage Springer-Verlag Berlin Heidelberg New York
ISBN 0-387-57280-5 2nd Edition Springer-Verlag New York Berlin Heidelberg

ISBN 3-540-17386-2 1. Auflage Springer-Verlag Berlin Heidelberg New York
ISBN 0-387-17386-2 1st Edition Springer-Verlag New York Berlin Heidelberg

Library of Congress Cataloging-in-Publication Data. Leo, William R., 1948- . Techniques for nuclear and particle physics experiments: a how-to approach / William R. Leo. – 2nd rev. ed. p. cm. Includes bibliographical references and index. ISBN 3-540-57280-5 (Berlin: alk. paper). – ISBN 0-387-57280-5 (New York: alk. paper) 1. Particles (Nuclear physics)–Technique. 2. Particles (Nuclear physics)–Experiments. 3. Nuclear physics–Technique. 4. Nuclear physics–Experiments. 5. Nuclear counters. I. Title. QC793.46.L46 1994 539.7'2'078–dc20 93-38494

Typesetting: K+V Fotosatz OmbH, D-64743 Beerfelden
Printing and Binding: Universitätsdruckerei H. Stürtz AG, D-97080 Würzburg

SPIN: 10061553 56/3140 - 5 4 3 2 1 0 - Printed on acid-free paper

The absorption cross section can then be simply calculated by

$$\sigma^a = \sigma_c - \sigma^s . \tag{2.112}$$

Another formula which we will make use of very often when discussing detectors is the energy distribution of the Compton recoil electrons. By substituting into the Klein-Nishina formula, one obtains

$$\frac{d\sigma}{dT} = \frac{\pi r_e^2}{m_e c^2 \gamma^2}\left[2 + \frac{s^2}{\gamma^2(1-s)^2} + \frac{s}{1-s}\left(s - \frac{2}{\gamma}\right)\right], \tag{2.113}$$

where $s = T/h\nu$. Figure 2.24 shows this distribution for several incident photon energies. The maximum recoil energy allowed by kinematics is given by

$$T_{max} = h\nu\left(\frac{2\gamma}{1+2\gamma}\right) \tag{2.114}$$

[see (2.106)] and is known as the Compton *edge*.

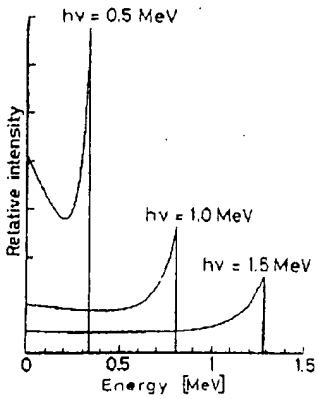

Fig. 2.24. Energy distribution of Compton recoil electrons. The sharp drop at the maximum recoil energy is known as the *Compton edge*

Thomson and Rayleigh Scattering. Related to Compton scattering are the classical processes of *Thomson* and *Rayleigh* scattering. Thomson scattering is the scattering of photons by free electrons in the classical limit. At low energies with respect to the electron mass, the Klein-Nishina formula, in fact, reduces to the Thomson cross-section,

$$\sigma = \frac{8\pi}{3} r_e^2 . \tag{2.115}$$

Rayleigh scattering, on the other hand, is the scattering of photons by atoms as a whole. In this process, all the electrons in the atom participate in a coherent manner. For this reason it is also called *coherent* scattering.

In both processes, the scattering is characterized by the fact that *no* energy is transferred to the medium. The atoms are neither excited nor ionized and only the direction of the photon is changed. At the relatively high energies of x-rays and γ-rays, Thomson and Rayleigh scattering are very small and for most purposes can be neglected.

2.7.3 Pair Production

The process of pair production involves the transformation of a photon into an electron-positron pair. In order to conserve momentum, this can only occur in the presence of a third body, usually a nucleus. Moreover, to create the pair, the photon must have at least an energy of 1.022 MeV.

Theoretically, pair production is related to bremsstrahlung by a simple substitution rule, so that once the calculations for one process are made, results for the other immediately follow. As for bremsstrahlung, the screening by the atomic electrons surrounding the nucleus plays an important role in pair production. The cross sections are thus dependent on the parameter ξ [see (2.67)], which is now defined by

$$\xi = \frac{100 m_e c^2 h\nu}{E_+ E_- Z^{1/3}} \tag{2.116}$$

with E_+: total energy of outgoing positron; E_-: total energy of outgoing electron.

At extreme relativistic energies and arbitrary screening, a Born approximation calculation gives the formula

$$d\tau = 4Z^2 r_e^2 \alpha \frac{dE_+}{(h\nu)^3}\left\{(E_+^2+E_-^2)\left[\frac{\phi_1(\xi)}{4}-\frac{1}{3}\ln Z - f(Z)\right] + \frac{2}{3}E_+E_-\left[\frac{\phi_2(\xi)}{4}-\frac{1}{3}\ln Z - f(Z)\right]\right\} \tag{2.117}$$

where ϕ_1 and ϕ_2 are the screening functions used in (2.69) and the other variables are as defined in (2.68).

As before, this formula simplifies in the limiting cases of no screening and complete screening. Thus for no screening ($\xi \gg 1$), we obtain

$$d\tau = 4Z^2\alpha r_e^2 dE_+ \frac{E_+^2+E_-^2+2E_+E_-/3}{(h\nu)^3}\left[\ln\frac{2E_+E_-}{h\nu m_e c^2}-\frac{1}{2}-f(Z)\right], \tag{2.118}$$

while for complete screening, $\xi \to 0$,

$$d\tau = 4Z^2\alpha r_e^2 \frac{dE_+}{(h\nu)^3}\left\{\left(E_+^2+E_-^2+\frac{2E_+E_-}{3}\right)[\ln(183Z^{-1/3})-f(Z)]-\frac{E_+E_-}{9}\right\}. \tag{2.119}$$

Because of the Born approximation, these formulae are not very accurate for high Z or low energy. A more complicated formula valid for low energies and no screening has been derived by Bethe and Heitler and is given in the article by *Bethe* and *Ashkin* [2.10] along with a somewhat simpler formula from Hough.

To obtain the total pair production cross section, a numerical integration of the above expressions must generally be performed. In the case of no screening with $m_e c^2 \ll h\nu \ll 137 m_e c^2 Z^{-1/3}$, an analytic integration is possible yielding

$$\tau_{\text{pair}} = 4Z^2\alpha r_e^2\left[\frac{7}{9}\left(\ln\frac{2h\nu}{m_e c^2}-f(Z)\right)-\frac{109}{54}\right]. \tag{2.120}$$

Similarly for complete screening, $h\nu \gg 137 m_e c^2 Z^{-1/3}$,

$$\tau_{\text{pair}} = 4Z^2\alpha r_e^2\{\tfrac{7}{9}[\ln(183Z^{-1/3})-f(Z)]-1/54\}. \tag{2.121}$$

For all other cases, a numerical integration of (2.117) must be performed. Figure 2.25 illustrates the energy dependence of the total pair cross section.

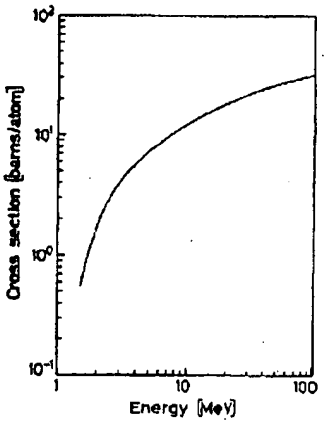

Fig. 2.25. Pair production cross section in lead

As for bremsstrahlung, pair production may also occur in the field of an atomic electron. Not surprisingly, a similar result is obtained for the cross section, but smaller by about a factor Z. To approximately account for this interaction, then, one need only replace Z^2 by $Z(Z+1)$ in the above formulae.

From the total cross section, it is interesting to calculate the mean free path, λ_{pair}, of a γ-ray for pair production. Thus, using (2.121)

$$1/\lambda_{\text{pair}} = N\tau_{\text{pair}} \simeq \tfrac{7}{9}\,4Z(Z+1)Nr_e^2\alpha[\ln(183Z^{-1/3})-f(Z)], \tag{2.122}$$

where N is the density of atoms and we have ignored the small constant term. This may be recognized as being very similar to the radiation length, and, in fact, comparison with (2.81) shows

$$\lambda_{\text{pair}} \simeq \tfrac{9}{7} L_{\text{rad}} . \tag{2.123}$$

2.7.4 Electron-Photon Showers

One of the most impressive results of the combined effect of pair production by high energy photons and bremsstrahlung emission by electrons is the formation of *electron-photon showers*. A high energy photon in matter converts into an electron and positron pair which then emit energetic bremsstrahlung photons. These, in turn, convert into further e^+e^- pairs, and so on. The result is a cascade or *shower* of photons, electrons and positrons. This continues until the energy of the pair-produced electrons and positrons drops below the critical energy. At this point, the e^+e^- pairs will preferentially lose their energy via atomic collisions rather than bremsstrahlung emission, thus halting the cascade.

The development of the cascade is, of course, a statistical process. Using the notion of radiation length, however, we may construct a simple model to describe the mean number of particles produced and their mean energies as a function of penetration depth in the converting material. Suppose we begin with an energetic photon of energy E_0. On the average, then, the photon will convert into an e^+e^- pair after one radiation length. The energy of each member of the pair is then $E_0/2$. After two radiation lengths, the electron and positron will then each emit a bremsstrahlung photon with approximately half the energy of the charged particle. At this point there are 4 particles present: two photons and an electron-positron pair, each with energy $E_0/4$. At the end of three radiation lengths, the bremsstrahlung photons will have converted into two more e^+e^- pairs, while the original pair will have emitted another set of bremsstrahlung photons. The number of particles present is thus 8 and their energy $E_0/8$. Continuing in this manner, it is easy to see that at the end of t radiation lengths, the total number of particles (i.e., photons, electrons and positrons) present will be

$$N = 2^t \tag{2.124}$$

each with an average energy of

$$E(t) = \frac{E_0}{2^t} . \tag{2.125}$$

The same result would also be obtained had we started with an electron rather than a photon.

Now what is the maximum penetration depth of the cascade? If we assume that the shower stops abruptly at the critical energy E_c, then, we have

$$E(t_{\max}) = \frac{E_0}{2^{t_{\max}}} = E_c \tag{2.126}$$

which, solving for $t_{\max}$, yields,

7. Scintillation Detectors

The *scintillation* detector is undoubtedly one of the most often and widely used particle detection devices in nuclear and particle physics today. It makes use of the fact that certain materials when struck by a nuclear particle or radiation, emit a small flash of light, i.e. a scintillation. When coupled to an amplifying device such as a photomultiplier, these scintillations can be converted into electrical pulses which can then be analyzed and counted electronically to give information concerning the incident radiation.

Probably the earliest example of the use of scintillators for particle detection was the spinthariscope invented by Crookes in 1903. This instrument consisted of a ZnS screen which produced weak scintillations when struck by α-particles. When viewed by a microscope in a darkened room, they could be discerned with the naked eye, although some practice was necessary. It was tedious to use, therefore, and thus never very popular, even though it was spectacularly employed by Geiger and Marsden in their famous α scattering experiments. Indeed, with the invention of the gaseous ionization instruments, the optical scintillation counter fell into quick disuse.

In 1944, not quite a half century later, Curran and Baker resuscitated the instrument by replacing the human eye with the then newly developed photomultiplier tube. The weak scintillations could now be counted with an efficiency and reliability equal to that of the gaseous ionization instruments. Thus was born the modern electronic scintillation detector. New developments and improvements followed rapidly so that by the mid-1950's scintillation detectors were among the most reliable and convenient available. This is still true today. In this chapter, we will survey the existing materials and current techniques in use as well as describe their basic underlying principles.

7.1 General Characteristics

The basic elements of a scintillation detector are sketched below in Fig. 7.1. Generally, it consists of a scintillating material which is optically coupled to a photomultiplier either directly or via a light guide. As radiation passes through the scintillator, it excites the atoms and molecules making up the scintillator causing light to be emitted. This

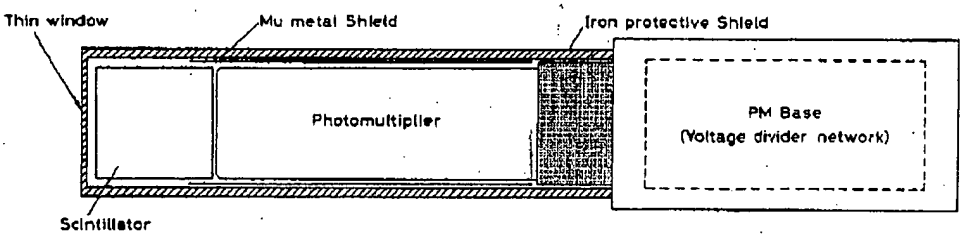

Fig. 7.1. Schematic diagram of a scintillation counter

light is transmitted to the photomultiplier (PM or PMT for short) where it is converted into a weak current of photoelectrons which is then further amplified by an electron-multiplier system. The resulting current signal is then analyzed by an electronics system.

In general, the scintillator signal is capable of providing a variety of information. Among its most outstanding features are:

1) *Sensitivity to Energy.* Above a certain minimum energy, most scintillators behave in a near linear fashion with respect to the energy deposited, i.e., the light output of a scintillator is directly proportional to the exciting energy. Since the photomultiplier is also a linear device, (when operated properly!), the amplitude of the final electrical signal will also be proportional to this energy. This makes the scintillator suitable as an energy spectrometer although it is not the ideal instrument for this purpose.
2) *Fast Time Response.* Scintillation detectors are fast instruments in the sense that their response and recovery times are short relative to other types of detectors. This faster response allows timing information, i.e., the time difference between two events, to be obtained with greater precision, for example. This and its fast recovery time also allow scintillation detectors to accept higher count rates since the dead time, i.e., the time that is lost while waiting for the scintillator to recover, is reduced.
3) *Pulse Shape Discrimination.* With certain scintillators, it is possible to distinguish between different types of particles by analyzing the shape of the emitted light pulses. This is due to the excitation of different fluorescence mechanisms by particles of different ionizing power. The technique is known as *pulse-shape discrimination* and is discussed in more detail later in this chapter.

Scintillator materials exhibit the property known as *luminescence.* Luminescent materials, when exposed to certain forms of energy, for example, light, heat, radiation, etc., absorb and reemit the energy in the form of visible light. If the reemission occurs immediately after absorption or more precisely within 10^{-8} s (10^{-8} s being roughly the time taken for atomic transitions), the process is usually called *fluorescence.* However, if reemission is delayed because the excited state is metastable, the process is called *phosphorescence* or *afterglow.* In such cases, the delay time between absorption and reemission may last anywhere from a few microseconds to hours depending on the material.

As a first approximation, the time evolution of the reemission process may be described as a simple exponential decay (Fig. 7.2)

$$N = \frac{N_0}{\tau_d} \exp\left(\frac{-t}{\tau_d}\right) , \tag{7.1}$$

where N is the number of photons emitted at time t, N_0 the total number of photons emitted, and τ_d the decay constant. The finite rise time from zero to the maximum in most materials is usually much shorter than the decay time and has been taken as zero here for simplicity.

While this simple representation is adequate for most purposes, some, in fact, exhibit a more complex decay. A more accurate description, in these cases, may be given by a two-component exponential

$$N = A \exp\left(\frac{-t}{\tau_f}\right) + B \exp\left(\frac{-t}{\tau_s}\right) , \tag{7.2}$$

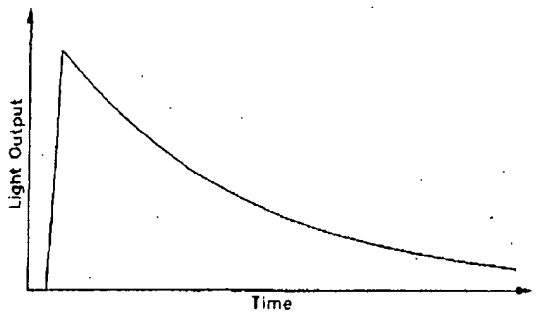

Fig. 7.2. Simple exponential decay of fluorescent radiation. The rise time is usually much faster than the decay time

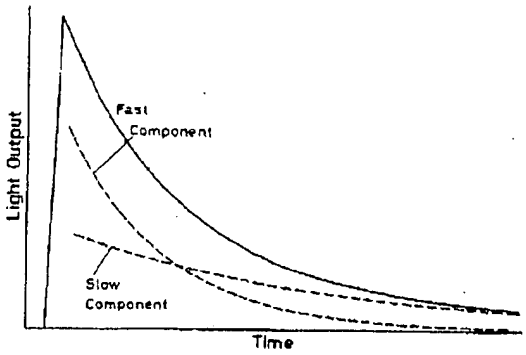

Fig. 7.3. Resolving scintillation light into *fast* (prompt) and *slow* (delayed) components. The *solid line* represents the total light decay curve

where τ_s and τ_f are the decay constants. For most scintillators, one component is generally much faster than the other so that it has become customary to refer to them as the *fast* and *slow* components (hence the subscripts f and s), or the *prompt* and *delayed* components. Their relative magnitudes, A and B, vary from material to material, although it is the fast component which generally dominates. Figure 7.3 shows the relation between these components. As will be seen in a later section, the existence of these two components forms the basis for the technique of pulse shape discrimination.

While many scintillating materials exist, not all are suitable as detectors. In general, a good detector scintillator should satisfy the following requirements:

1) high efficiency for conversion of exciting energy to fluorescent radiation
2) transparency to its fluorescent radiation so as to allow transmission of the light
3) emission in a spectral range consistent with the spectral response of existing photomultipliers
4) a short decay constant, τ.

At present, six types of scintillator materials are in use: organic crystals, organic liquids, plastics, inorganic crystals, gases and glasses. In the following sections we will briefly describe each category. Their basic properties are summarized in Table 7.1.

7.2 Organic Scintillators

The organic scintillators are aromatic hydrocarbon compounds containing linked or condensed benzene-ring structures. Their most distinguishing feature is a very rapid decay time on the order of a few nanoseconds or less.

Scintillation light in these compounds arises from transitions made by the *free* valence electrons of the molecules. These delocalized electrons are not associated with any particular atom in the molecule and occupy what are known as the *π-molecular orbitals*. A typical energy diagram for these orbitals is shown in Fig. 7.4, where we have distinguished the spin singlet states from the spin triplet states. The ground state is a singlet state which we denote by S_0. Above this level are the excited singlet states (S^*, S^{**}, ...) and the lowest triplet state (T_0) and its excited levels (T^*, T^{**}, ...). Also associat-

Table 7.1. Physical properties of various commercial scintillators (data from Nuclear Enterprises scintillator catalog [7.1])

	Scintillator	Type	Density	Refractive index	Melting softening or boiling point C[a]	Light output (% Anthracene)	Decay constant, main component [ns]	Wavelength of maximum emission [nm]	Content of loading element (% by wt.)	H/C No. of H atoms/ No. of C atoms	Principal applications
Plastic	NE 102A	Plastic	1.032	1.581	75	65	2.4	423		1.104	γ, α, β, fast n
	NE 104	Plastic	1.032	1.581	75	68	1.9	406		1.100	ultra-fast counting
	NE 104B	Plastic	1.032	1.58	75	59	3.0	406		1.107	with BBQ light guides
	NE 105	Plastic	1.037	1.58	75	46		423		1.098	dosimetry
	NE 110	Plastic	1.032	1.58	75	60	3.3	434		1.104	γ, α, β, fast n etc.
	NE 111A	Plastic	1.032	1.58	75	55	1.6	370		1.103	ultra-fast timing
	NE 114	Plastic	1.032	1.58	75	50	4.0	434		1.109	as for NE 110
	NE 160	Plastic	1.032	1.58	80	59	2.3	423		1.105	use at high temperatures
	Pilot U	Plastic	1.032	1.58	75	67	1.36	391		1.100	ultra fast timing
	Pilot 425	Plastic	1.19	1.49	100			425		1.6	Cherenkov detector
Liquid	NE 213	Liquid	0.874	1.508	141	78	3.7	425		1.213	fast n (P.S.D.)
	NE 216	Liquid	0.885	1.523	141	78	3.5	425		1.171	α, β (internal counting)
	NE 220	Liquid	1.036	1.442	104	65	3.8	425	O 29%	1.669	internal counting, dosimetry
	NE 221	Gel	1.08	1.442	104	55	4	425		1.669	α, β (internal counting)
	NE 224	Liquid	0.877	1.505	169	80	2.6	425		1.330	γ, fast n
	NE 226	Liquid	1.61	1.38	80	20	3.3	430		0	γ, insensitive to n
	NE 228	Liquid	0.71	1.403	99	45		385		2.11	n
	NE 230	Deuterated liquid	0.945	1.50	81	60	3.0	425	D 14.2%	0.984	(D/C) special applications
	NE 232	Deuterated liquid	0.89	1.43	81	60	4	430	D 24.5%	1.96	(D/C) special applications
	NE 233	Liquid	0.874	1.506	117	74	3.7	425		1.118	α, β (internal counting)
	NE 235	Liquid	0.858	1.47	350	40	4	420		2.0	large tanks
	NE 250	Liquid	1.035	1.452	104	50	4	425	O 32%	1.760	internal counting, dosimetry
Loaded liquid	NE 311 & 311A	B loaded liquid	0.91	1.411	85	65	3.8	425	B 5%	1.701	n, β
	NE 313	Gd loaded liquid	0.88	1.506	136	62	4.0	425	Gd 0.5%	1.220	n
	NE 316	Sn loaded liquid	0.93	1.496	148.5	35	4.0	425	Sn 10%	1.411	γ, x-rays
	NE 323	Gd loaded liquid	0.879	1.50	161	60	3.8	425	Gd 0.5%	1.377	n
					110	300	200	450	Li 5%		slow n

Neutron (ZnS-type) and glass	NE 422 & 426	^{6}Li-ZnS(Ag)	2.36		110	300	200	450	Li 5%		slow *n*
	NE 451	ZnS(Ag) plastic	1.443		110	300	200	450			fast *n*
	NE 901, 902, 903	Glass	2.64	1.58	c. 1200	28	20 & 60	395	Li 2.3%		*n*, β
	NE 904, 905, 906	Glass	2.5	1.55	c. 1200	25	20 & 58	395	Li 6.6%		*n*
	NE 907, 908	Glass	2.42	1.566	c. 1200	20	18 & 62	399	Li 7.5%		*n*
	NE 912, 913	Glass	2.3	1.55	c. 1200	25	18 & 55	397	Li 7.7%		*n*, β (low background)
Crystal	Anthracene	Crystal	1.25	1.62	217	100	30	447		0.715	γ, α, β, fast *n*
	Stilbene	Crystal	1.16	1.626	125	50	4.5	410		0.858	fast *n* (P.S.D.), γ, etc.
	NaI(Tl)	Crystal	3.67	1.775	650	230	230	413			γ, x-rays
	NaI(pure)	Crystal	3.67	1.775	651	440[b]	60[b]	303[b]			γ, x-rays (fast counting)
	LiI(Eu)	Crystal	4.06	1.955	445	75	1200	475			*n*
	CsI(Tl)	Crystal	4.51	1.788	620	95	1100	580			heavy particles, γ (P.S.D.)
	CsI(Na)	Crystal	4.51	1.787	621	150.190	650	420			heavy particles, γ (P.S.D.)
	CsI(pure)	Crystal	4.51	1.788	621	500[b]	600[b]	c. 400[b]			heavy particles, γ (low energy)
	CaF_2(Eu)	Crystal	3.17	1.443	1418	110	1000	435			β, x-rays etc.
	$CaWO_4$	Crystal	6.1	1.92	1535	36	6000	430			γ (seldom used)
	ZnS(Ag)	Multi-crystal	4.09	2.356	1850	300	200	450			α
	ZnO(Ga)	Multi-crystal	5.61	2.02	1975	90	1.48	385			α

[a] Although NE 160 begins to soften very slightly at approximatley 80 °C, it retains its shape up to at least 150 °C unlike other plastic scintillators as NE 102A.
[b] At liquid nitrogen temperature.

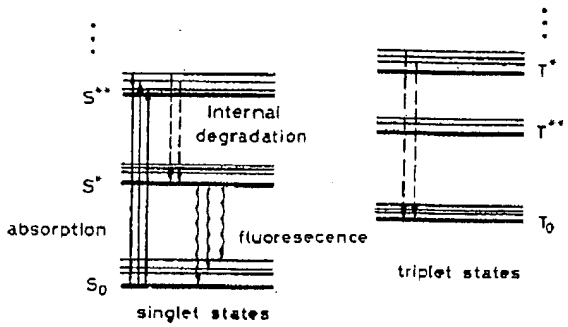

Fig. 7.4. Energy level diagram of an organic scintillator molecule. For clarity, the singlet states (denoted by S) are separated from the triplet states (denoted by T)

ed with each electron level is a fine structure which corresponds to excited vibrational modes of the molecule. The energy spacing between electron levels is on the order of a few eV whereas that between vibrational levels is of the order of a few tenths of eV.

Ionization energy from penetrating radiation excites both the electron and vibrational levels as shown by the solid arrows. The singlet excitations generally decay immediately (≤ 10 ps) to the S^* state without the emission of radiation, a process which is known as *internal degradation*. From S^*, there is generally a high probability of making a radiative decay to one of the vibrational states of the ground state S_0 (wavy lines) within a few nanoseconds time. This is the normal process of fluorescence which is described by the *prompt* exponential component in (7.2). The fact that S^* decays to excited vibrational states of S_0, with emission of radiation energy less than that required for the transition $S_0 \rightarrow S^*$ also explains the transparency of the scintillators to their own radiation.

For the triplet excited states, a similar internal degradation process occurs which brings the system to the lowest triplet state. While transitions from T_0 to S_0 are possible, they are, however, highly forbidden by multipole selection rules. The T_0 state, instead, decays mainly by interacting with another excited T_0 molecule,

$$T_0 + T_0 \rightarrow S^* + S_0 + \text{phonons} \tag{7.3}$$

to leave one of the molecules in the S^* state. Radiation is then emitted by the S^* as described above. This light comes after a delay time characteristic of the interaction between the excited molecule and is the *delayed* or *slow* component of scintillator light. The contribution of this slow component to the total light output is only significant in certain organic materials, however.

Because of the molecular nature of luminescence in these materials, organics can be used in many physical forms without the loss of their scintillating properties. As detectors, they have been used in the form of pure crystals and as mixtures of one or more compounds in liquid and solid solutions. A brief description of these types is given below.

7.2.1 Organic Crystals

The most common crystals are anthracene ($C_{14}H_{10}$), trans-stilbene ($C_{14}H_{12}$) and naphthalene ($C_{10}H_8$). With the exception of anthracene which has a decay time of $\simeq 30$ ns, these crystals have a fast time response on the order of a few nanoseconds. However,

due to channeling effects their amplitude response is anisotropic, that is, for a constant source of radiation the response varies with the orientation of the crystal. Obtaining a good energy resolution with a noncollimated source, then, can become a difficult problem.

They are hard crystals and thus very durable, although stilbene tends to be brittle and more sensitive to thermal shock than anthracene. For this reason also, the cutting of such crystals to desired forms and shapes is often a difficult task. This and other disadvantages, unfortunately, have caused anthracene and stilbene to fall into disuse in the past years.

Anthracene, nevertheless, has the distinction of having the highest light output of all the organic scintillators. For this reason, it is chosen as the reference to which the light outputs of other scintillators are compared. These outputs are thus usually expressed as percent of anthracene light.

7.2.2 Organic Liquids

These materials are liquid solutions of one or more organic scintillators in an organic solvent. While the scintillation process here is still the same as that described above, the mechanism of energy absorption is different. In solutions, the ionization energy seems to be absorbed mainly by the solvent and then passed on to the scintillation solute. This transfer usually occurs very quickly and efficiently, although the precise details of the mechanism are still not clear.

Some of the organic scintillators most commonly used as solutes are p-Terphenyl[1], PBD[2], PPO[3] and POPOP[4]. Among the solvents, the most successful seem to be xylene, toluene, benzene, phenylcyclohexane, triethylbenzene and decaline. Measurements have shown that the efficiency of liquid scintillators increases with solute concentration although a broad maximum is reached just before saturation of the solution. Typical concentrations are on the order of 3 g of solute per liter of solvent.

The response of liquid scintillators is generally quite fast with decay times on the order of 3 to 4 ns. They have a particular advantage in that they can be easily *loaded* with other materials so as to increase efficiency for a particular application. For example, Boron-11, which has a high neutron cross-section, can be added to increase efficiency for neutron detection. Similarly, *wavelength shifters*, i.e. materials which absorb light of one frequency and reemit it at another, can also be added to make the spectrum of emitted light more compatible with a photomultiplier cathode. Loading, however, usually causes a lengthening of the decay time and a drop in light output because of a quenching effect which is produced by these additives. It has been found, though, that by adding naphthalene, biphenyl and other compounds to the solvent, much of the quenching effect can be removed.

As a general rule, liquid scintillators are extremely sensitive to impurities in the solvent. It is not uncommon, in fact, to find two different samples of the same liquid scintillator with pulse heights differing by as much as a factor of 2 because of contaminating impurities. Dissolved oxygen, in particular, seems to have a large effect, although

[1] $C_{18}H_{14}$
[2] 2-phenyl,5-(4-biphenylyl)-1,3,4-oxadiazole ($C_{20}H_{14}N_2O$)
[3] 2,5-diphenyloxazole ($C_{15}H_{11}NO$)
[4] 1,4-Bis-[2-(5-phenyloxazolyl)]-benzene ($C_{24}H_{16}N_2O_2$)

this problem can be remedied to some extent by bubbling oxygen-free nitrogen through the liquid scintillator.

7.2.3 Plastics

In nuclear and particle physics, plastic scintillators are probably the most widely used of the organic detectors today. Like the organic liquids, plastic scintillators are also solutions of organic scintillators but in a solid plastic solvent. The most common and widely used plastics are polyvinyltoluene, polyphenylbenzene and polystyrene. Some common primary solutes are PBD, p-Terphenyl and PBO, which are dissolved in concentrations typically on the order of 10 g/l. Very often a secondary solute such as POPOP is also added for its wavelength shifting properties, but in a very much smaller proportion. The light emission spectra of several commercial plastics is shown in Fig. 7.5.

Plastics offer an extremely fast signal with a decay constant of about 2 – 3 ns and a high light output. Because of this fast decay, the finite rise time cannot be ignored in the description of the light pulse as was done in (7.1). The best mathematical description, as shown by *Bengston* and *Moszynski* [7.2], appears to be the convolution of a Gaussian with an exponential,

$$N(t) = N_0 f(\sigma, t) \exp\left(\frac{-t}{\tau}\right), \tag{7.4}$$

where $f(\sigma, t)$ is a Gaussian with a standard deviation σ. Table 7.2 gives some fitted values of these parameters for a few common plastics.

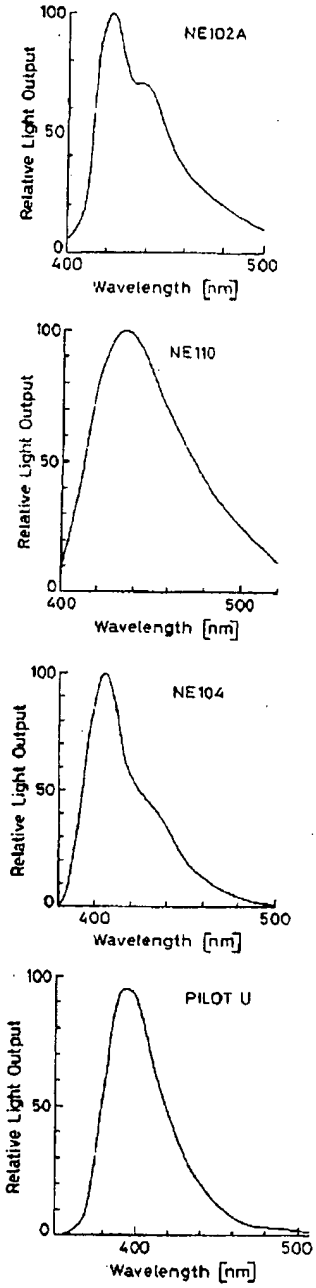

Fig. 7.5. Light emission spectra for several different plastic scintillators (from *Nuclear Enterprises* catalog [7.1])

Table 7.2. Gaussian and exponential parameters for light pulse description from several plastic scintillators (from *Bengston* and *Moszynski* [7.2])

Scintillator	σ [ns]	τ [ns]
NE102A	0.7	2.4
NE111	0.2	1.7
Naton 136	0.5	1.87

One of the major advantages of plastics is their flexibility. They are easily machined by normal means and shaped to desired forms. They are produced commercially in a wide variety of sizes and forms, ranging from thin films, a few $\mu g/cm^2$ thick, to large sheets, blocks and cylinders, and are relatively cheap. Moreover, various types of plastics are made offering differences in light transmission, speed, etc.

While they are generally quite rugged, plastics are easily attacked by organic solvents such as acetone and other aromatic compounds. They are, however, resistant to water pure methylal (dimethoxymethane), silicone grease and lower alcohols. When handling unprotected plastic, it is generally advisable to wear cotton or terylene gloves as the body acids from one's hands can cause a cracking of the plastic (often referred to as *craze*) after a period of time.

Introduction to experimental particle physics

RICHARD C. FERNOW
Physics Department
Brookhaven National Laboratory

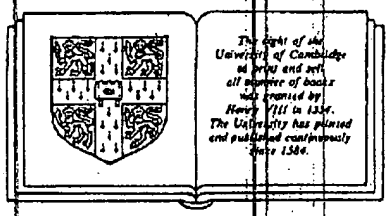

CAMBRIDGE UNIVERSITY PRESS
Cambridge
New York Port Chester
Melbourne Sydney

Published by the Press Syndicate of the University of Cambridge
The Pitt Building, Trumpington Street, Cambridge CB2 1RP
40 West 20th Street, New York, NY 10011, USA
10 Stamford Road, Oakleigh, Melbourne 3166, Australia

First published 1986
First paperback edition 1989
Reprinted 1990

Printed in the United States of America

Library of Congress Cataloging in Publication Data
Fernow, Richard C. (Richard Clinton), 1947–
Introduction to experimental particle physics.
Includes indexes.
1. Particles (Nuclear physics) – Experiments.
2. Particles (Nuclear physics) – Technique.
3. Nuclear counters. 4. Nuclear reactions.
5. Electromagnetic interactions. I. Title.
QC793.2.F47 1986 539.7'21 85–14931

British Library Cataloguing in Publication Data
Fernow, Richard C.
Introduction to experimental particle physics.
1. Particles (Nuclear physics)
I. Title
539.7'21 QC793.2

ISBN 0-521-30170-X hardback
ISBN 0-521-37940-7 paperback

is 6.2 ± 1.2 muons/day-m^2, a reduction of about 10^6 of the flux at sea level [19]. The outer layer of the detector is used to veto muons coming in from outside the detector. Good nucleon decay events must originate in the fiducial volume of the detector. On the other hand, the neutrino flux is largely unaffected by attenuation in the earth and enters the detector from all directions, regardless of depth. A neutrino interaction inside the fiducial volume may look like a nucleon decay, and this limits the ultimate sensitivity of the experiments.

14.6 Data acquisition

A large detector system is capable of generating immense amounts of digital and analog signals. It is the function of the data acquisition system to control the flow of this information. In general, it is desirable to at least monitor the performance of the experiment as it is happening (online) and to save some of the data for subsequent (offline) analysis. A minimal system for a simple experiment would likely use CAMAC modules as the interface between the experimental equipment and a small computer.

Most experiments make use of a minicomputer to control the online monitoring and data collection for the experiment [21]. Figure 14.13 shows a typical online data acquisition system for a more complicated experiment. The data acquisition system is intimately connected with the trigger. Two constraints may require a highly selective trigger. First, with present technology no more than 10 – 100 events/sec can be handled and stored on permanent memory. Second, the offline data analysis may require ~ 1 sec/event so that the cost and availability of computer time may restrict the total number of events that can be processed.

The fast trigger detectors include devices such as scintillation counters, Cerenkov counters, and MWPCs. The signals are fed into the trigger logic, where discriminators standardize the pulses, and coincidence units indicate temporal correlations of signals from different detectors. If a good event has occurred, a fast trigger pulse is generated within a few hundred nanoseconds of the event. This causes other triggered devices such as drift chambers, ADCs, and TDCs to be read out.

All of the data is fed into some device that prepares the data in a recognizable fashion and channels it onto a pathway to the computer. Some systems may have a higher level trigger that can make a more complicated decision based on hodoscope matrix correlations or coarse track finding within about 1 μs. Still more complicated decisions may be made using hardware processors or dedicated minicomputers. Some-

Mt. Blanc	Italy–France	4270	30 tons iron and liquid Sc	PMT, streamer chamber

[a] MWe = Meters of water equivalent.
Source: Particle Data Group, Major detectors in elementary particle physics, LBL-91, UC-37, 1983; S. Weinberg, Sci. Amer., June 1981, p. 64; J. M. Lo Secco, F. Raines, and D. Sinclair, Sci. Amer., June 1985, p. 54.

times these special purpose devices have been designed to emulate the instruction set of a larger, more powerful computer [22]. Then the online filtering program can first be thoroughly tested using the large computer before being used for an experiment. The emulator is slower than the large computer but is much cheaper.

Since the events occur randomly, it may be necessary to provide some temporary storage media or buffer that can store the data from one event while the detector and trigger logic are examining another one. The buffer holds the data until the online computer finishes processing an event and makes the data available for writing onto magnetic tape, at which point it is ready to accept the data from another event. If the trigger rate, computer processing rate, and buffer capabilities are not carefully balanced, many events may occur while the data acquisition system is busy processing a preceding event.

A more sophisticated data acquisition system for a large experiment is outlined in Table 14.8. At the LEP storage ring 25 μs will be available

Figure 14.13 A data acquisition system.

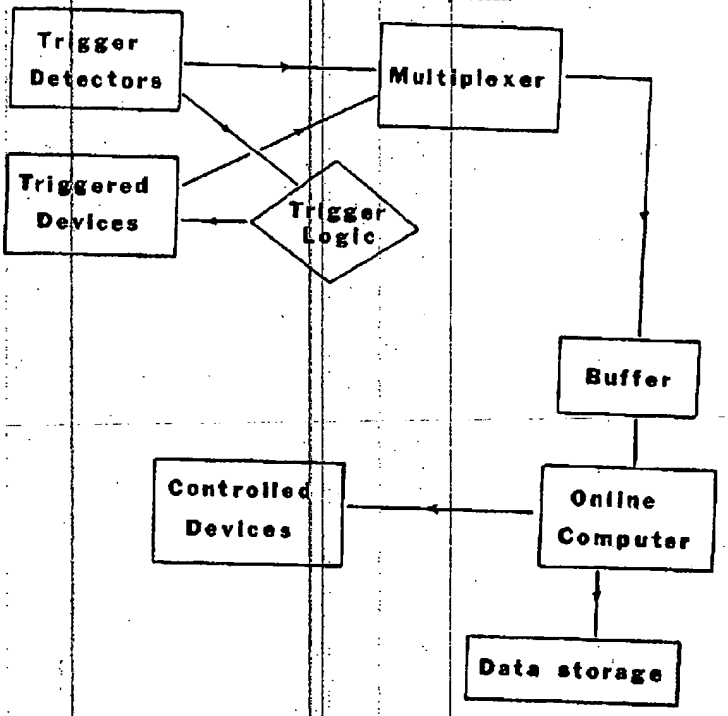

e been designed to emulate the
i computer [22]. Then the online
· tested using the large computer
· emulator is slower than the large

ıay be necessary to provide some
ıan store the data from one event
amining another one. The buffer
· finishes processing an event and
› magnetic tape, at which point it
vent. If the trigger rate, computer
ıre not carefully balanced, many
ition system is busy processing a

ı system for a large experiment is
rage ring 25 μs will be available

stem.

Table 14.8. *Data acquisition flow*

Level		Characteristic time	Equipment	Data treatment
1	fast trigger	0.1–25 μs	NIM electronics; fast correlation matrices	trigger detector signals, rough topology
2	detector readout	0.025–3 ms	programmable processors using integer arithmetic	drift chambers, analog signals; suppression of empty channels, clusters
3	transfer to computer	5–25 ms	floating point processors, emulator	calculate track vectors, particle reconstruction
4	data recording	0.025–1 sec	minicomputer	filtering based on full event reconstruction

Source: R. Dobinson, Physica Scripta 23: 487, 1981.

between bunch crossings. Assuming that there is only a small probability for more than one interaction per bunch crossing, trigger decisions that can be made in less than 25 μs will not introduce any deadtime. At each of the higher levels the event selection can be refined. Only the data for events that reach level 4 are recorded [23].

The online computer can perform various auxiliary functions. Analog measuring devices must be calibrated [24]. This generally requires operating the detector in a test beam or under special conditions or injecting a known test signal and measuring the detector's response.

Monitoring of the detectors is a second important auxiliary function of the online computer [24]. The monitoring can be passive, in the sense that the software merely histograms channel hit frequencies and calculates distributions at the same time that the experiment is taking data. Generally this works adequately, so long as sufficient statistics are accumulated for all channels in a reasonable length of time. Otherwise an active monitoring system may be required. An active system injects a test signal as early as possible into the detector elements and then checks that the detectors return the correct response.

Some examples of specific tasks for the monitoring software include checking the high voltages on power supplies, currents in magnets, and scaler contents. This information can be used as part of a feedback loop to adjust the settings of tuneable devices.

References

[1] R. Gluckstern, Uncertainties in track momentum and direction due to multiple scattering and measurement errors, Nuc. Instr. Meth. 24: 381–9, 1963.
[2] K. Amako, K. Kawano, S. Sugimoto, and T. Matsui, High precision field measuring system for a large aperture spectrometer magnet, Nuc. Inst. Meth. 197: 325–30, 1982.
[3] C. Akerlof, R. Hieber, A. Krisch, K. Edwards, L. Ratner, and K. Ruddick, Elastic proton-proton scattering at 90° and structure within the proton, Phys. Rev. 159: 1138–49, 1967.
[4] Some examples of selecting detectors for specific types of e^+e^- physics studies are given in K. Winter, Some detector arrangements at LEP, Physica Scripta 23: 569–78, 1981.
[5] W. Panofsky, The evolution of SLAC and its program, Phys. Today, October, 1983, pp. 34–41.
[6] W. Willis, The large spectrometers, Phys. Today, October 1978, pp. 32–9.
[7] T. Taylor, The choice of spectrometer magnets for LEP, Physica Scripta 23: 459–64, 1981.
[8] D. Anderson, G. Charpak, Ch. Von Gagern, and S. Majewski, Recent developments in BaF_2 scintillator coupled to a low pressure wire chamber, Nuc. Inst. Meth. 225: 8–12, 1984.
[9] Particle Data Group, Major detectors in elementary particle physics, LBL-91, Supplement, UC-37, March 1983.

PHYSICAL REVIEW VOLUME 132, NUMBER 6 15 DECEMBER 1963

Inelastic Proton Scattering on Holmium-165 and Gadolinium-156*

A. LIEBER† AND C. A. WHITTEN
Palmer Physical Laboratory, Princeton University, Princeton, New Jersey
(Received 9 July 1963)

Elastic and inelastic scattering of 17.5-MeV protons by the low-lying rotational levels of holmium-165 and gadolinium-156 has been studied using a telescopic array of solid-state detectors with a resolution of about 60 keV. Angular distributions were obtained for the ground state ($7/2^-$), first excited state ($9/2^-$), and second excited state ($11/2^-$) of holmium-165, and the ground state (0^+), first excited state (2^+), and second excited state (4^+) of gadolinium-156. The cross section for the first excited state of Ho^{165} is an order of magnitude below that of the ground state. The ratio of the first excited state of Ho^{165} to that of the second does not agree with the prediction given by first-order direct reaction theory. There is some evidence that the third excited state of Gd^{156} (6^+) is weakly excited by 17.5-MeV protons.

I. INTRODUCTION

IN recent years a great deal of interest has been focused on the understanding of the elastic and inelastic scattering of medium-energy particles from nuclei. Distorted-wave theory[1–3] has been quite successful in fitting a wide variety of inelastic scattering reactions.[4–9] The simpler inelastic diffraction model,[10,11] which makes use of the Fraunhofer approximation, has enjoyed equivalent success in describing (α,α') reactions, but has been less applicable to (p,p') reactions.[12]

Because of resolution difficulties, most experimental investigations have been limited to light or medium-A nuclei, where the discussion of nuclear transitions in terms of a collective model is not necessarily justified. However, some recent work in the $A=60$ region has been extremely well explained in terms of a simple collective model.[13–15] With the advent of high resolution surface-barrier detectors capable of stopping 18-MeV protons, it is now possible to investigate the inelastic scattering of protons from high-A nuclei which are well known to be nonspherical rotors. Using a newly designed beam analyzing system in conjunction with high resolution detectors it has been possible to attain a total resolution of approximately 60 keV which is sufficient to resolve the low-lying excited states of rare-earth nuclei. In addition to obtaining angular distributions and cross sections for the inelastic states, we are also able to obtain elastic differential cross sections which are free from excited state contamination. These measurements then serve as a check on the survey elastic scattering data which had been used in optical-model analysis.[16]

II. EXPERIMENTAL PROCEDURE

The experiment was performed using the 17.5-MeV proton beam of the Princeton FM cyclotron.[17] The external beam system is shown in Fig. 1. The beam was first focused on a $\frac{1}{16}$-in. graphite slit with a quadrupole set and a steering magnet. A feedback system between this slit system and the steering magnet insured that the maximum intensity of the beam profile passed through the slit. This slit served as an object for a double focusing spectrometer magnet whose dispersion made it possible to analyze the beam to better than 35 keV using $\frac{1}{16}$-in. collimators. Beam currents were typically $2-3\times10^{-9}$ A. The experiment was carried out in a 20-in.-i.d. scattering chamber which was designed expressly for use with solid-state detectors, and which will be described elsewhere.[18] The beam was monitored and integrated using a model A310B Elcor integrator. A pressure of better than 10^{-5} mm Hg in the region of the scattering chamber insured accurate charge collection. Elastic cross sections for O^{16} have checked within 5% with measurements made by other experimentalists in a separate experimental setup.[19]

A sectional view of the detector used in this investigation is shown in Fig. 2. It consists of a telescope composed of two solid-state surface barrier detectors. The first detector is a fully depleted 1000-μ transmission mounted detector whose active area is $\frac{1}{4}$-in. diameter.[20] The second detector is a 1400-μ detector whose active

* This work was supported by the U. S. Atomic Energy Commission and the Higgins Scientific Trust Fund.
† Present address: Ames Research Center, Division of National Aeronautics and Space Administration, Moffett Field, California.
[1] R. H. Bassel, G. R. Satchler, R. M. Drisko, and E. Rost, Phys. Rev. 128, 2693 (1962).
[2] E. Rost, Phys. Rev. 128, 2708 (1962).
[3] J. Blair and N. Austern (to be published).
[4] D. R. Sweetman and N. S. Wall, *C. R. Congress on the International Physics of Nuclei* (Dunod, Paris, 1959), p. 549.
[5] H. W. Fulbright, N. O. Lassen, and Roy Poulsen Kgl. Danske Videnskab. Selskab, Mat. Fys. Medd. 31, No. 10 (1959).
[6] D. K. McDaniels, J. S. Blair, S. W. Chen, and G. W. Farwell, Nucl. Phys. 17, 614 (1960).
[7] J. L. Yntema and B. Zeidman, Phys. Rev. 114, 815 (1959).
[8] B. L. Cohen and A. G. Rubin, Phys. Rev. 111, 1568 (1958).
[9] C. Hu, K. Kiluchi, S. Kobayashi, K. Matsuda, Y. Nagahara, Y. Oda, N. Takuno, M. Takeda, and A. T. Yamazaki, J. Phys. Soc. Japan 14, 861 (1959).
[10] J. S. Blair, Phys. Rev. 115, 928 (1959).
[11] J. S. Blair, D. Sharp, and L. Wilets, Phys. Rev. 125, 1625 (1962).
[12] C. Levinson and M. Banerjee, Ann. Phys. 2, 471 (1957).
[13] N. R. Roberson and H. O. Funsten (to be published).
[14] F. Perey, R. J. Silva, and G. R. Satchler, Phys. Letters 4, 25 (1963).
[15] B. Buck, Phys. Rev. 130, 712 (1963).
[16] I. E. Dayton and G. Schrank, Phys. Rev. 101, 1358 (1956).
[17] J. L. Yntema and M. G. White, Phys. Rev. 95, 1226 (1954).
[18] A. Lieber, Nucl. Instr. Methods (to be published).
[19] W. W. Daehnick (to be published).
[20] Molychem, Incorporated, Pennington, New Jersey.

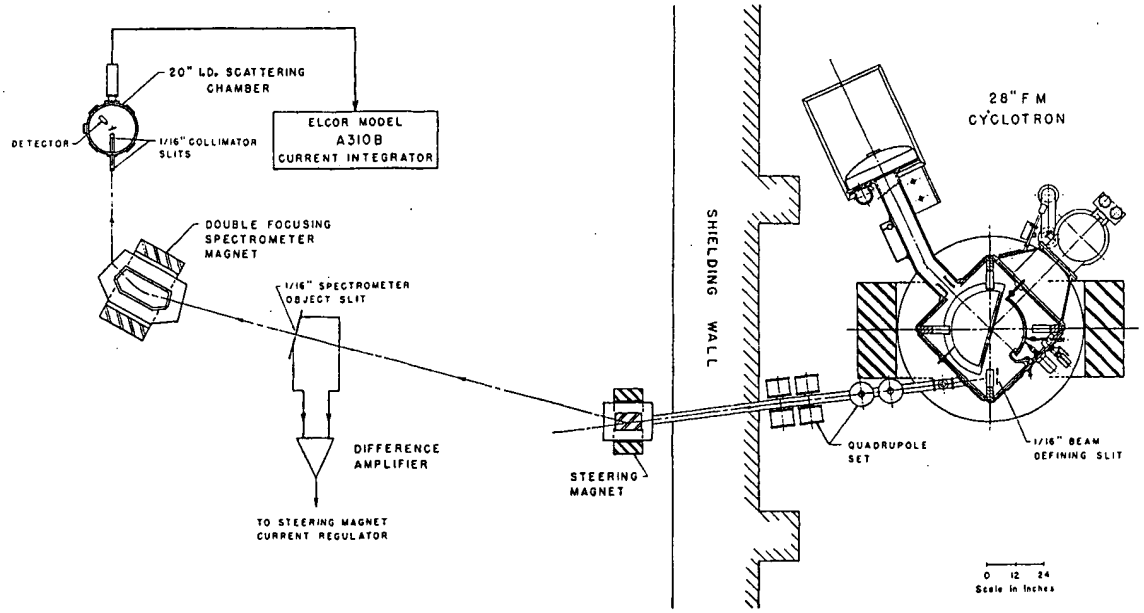

FIG. 1. Plan view of the external beam system of the Princeton FM cyclotron. The beam is collimated inside the cyclotron, focused on a graphite slit system and analyzed to better than 35 keV by a double focusing spectrometer magnet.

area is $\frac{5}{8}$-in. diameter.[21] In order to lower noise levels in these detectors the system was cooled using two thermoelectric diodes. These diodes are capable of maintaining a no load differential of 55°C between their plates, and in this configuration cooled the detectors to approximately −20°C. The collimators were constructed of nickel because of its low (p,n) cross section. They were tapered slightly to lower slit scattering and to remove

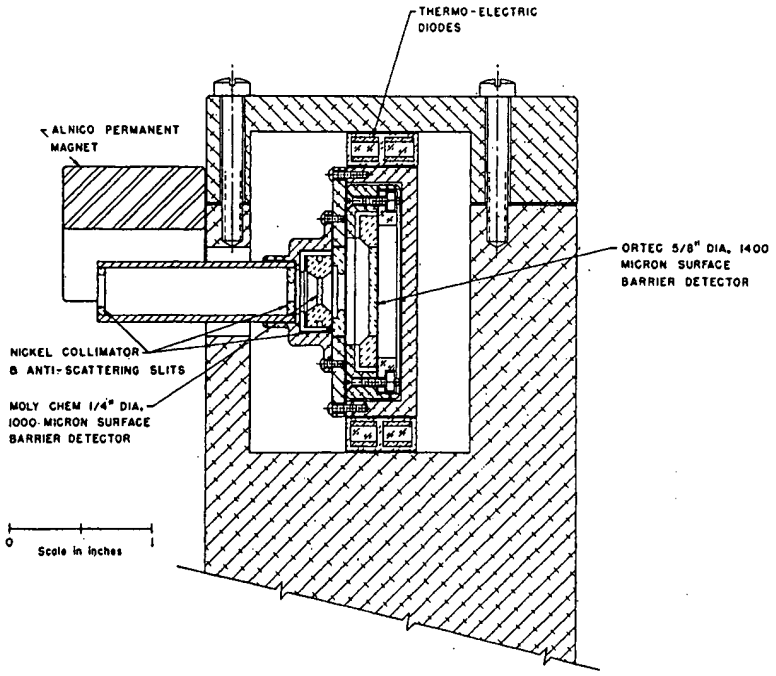

FIG. 2. Sectional view of the tandem solid-state telescope. The detectors are cooled by two thermoelectric diodes placed above and below the detector assembly. The outer aluminum body serves as a heat sink. Nickel collimators are employed to define the detectors solid angle and eliminate scattering because of their low (p,n) cross section.

[21] Kindly lent for evaluation by Oak Ridge Technical Enterprises, Incorporated, Oak Ridge, Tennessee.

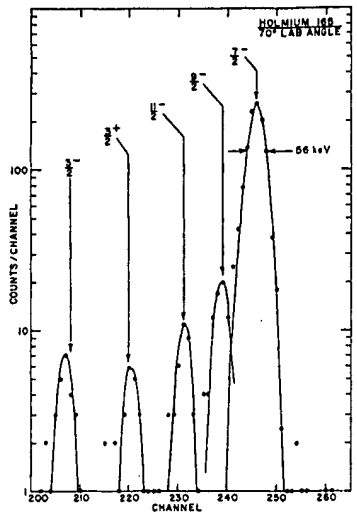

FIG. 3. Typical holmium-165 spectrum taken at 70°.

tails on the elastic peaks. A permanent Alnico magnet was used in front of the detector to sweep electrons away.

The signals derived from these two solid-state detectors were added and fed into a model 101-201 Ortec amplifier system. The data were displayed on a RIDL 400-channel analyzer. Typical resolution for the Ho^{165} target was 56-keV full width at half-maximum, while the resolution was 65-keV full width at half-maximum for the Gd^{156} target.

The discrepancy in resolutions for Ho^{165} and Gd^{156} spectra is due to the type of target used. The holmium target was prepared by evaporating the metal onto a 0.25-mil Polyethylene backing. Natural holmium is isotopically pure. The gadolinium target was prepared by evaporating an aqueous slurry of Gd_2O_3 on a 0.25-mil Polyethylene backing. Thus this target contained a known amount of oxygen which could serve as a check on cross sections and also serve as an aid in normalization. The Gd^{156} was obtained from Oak Ridge National Laboratories as a separated isotope. A spectral analysis of this sample showed it to be 97% Gd^{156}. The most abundant other isotope of gadolinium was Gd^{157} (1.2%) and the largest trace of other rare earths was that of cerium (0.5%).

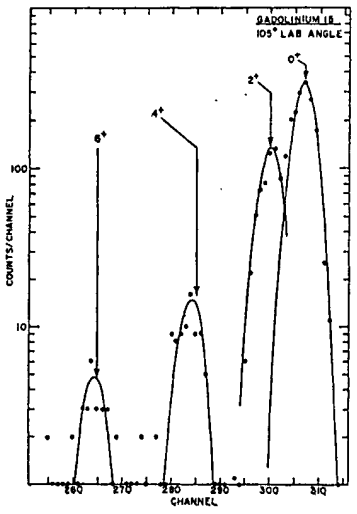

FIG. 4. Typical gadolinium-156 spectrum taken at 105°.

The spectra were plotted and Gaussians fitted to the peaks as an aid in peak separation. Typical spectra for holmium and gadolinium appear in Figs. 3 and 4, respectively. The oxygen ground state did not interfere with the region of interest for scattering angles greater than 35°, due to kinematics. In general, background subtractions for angles greater than 45° were unnecessary. It is felt that the largest source of error in determination of the cross sections for the excited states of holmium and gadolinium stems from unfolding the peaks.

III. EXPERIMENTAL RESULTS AND DISCUSSION

A. Holmium-165

Angular distributions for the ground state ($7/2^-$), first excited state ($9/2^-$), and second excited state ($11/2^-$) are shown in Fig. 5. Even though there is an indication of excited states up to the $3/2^-$ level in holmium in Fig. 3, the levels beyond the $11/2^-$ state were generally too weakly excited for angular distributions to be obtained. The error bars in Fig. 5 reflect the statistical uncertainties as well as a liberal allowance for errors incurred in unfolding the peaks. The function of the curves drawn in is to merely delineate the peaks.

One noteworthy feature of the angular distributions is that they all peak in the forward direction. Another is that the excited states have cross sections an order of magnitude below that for the ground state. Because of the difficulties in unfolding the first excited state from that of the ground state it would probably be unwise to attach too much significance to the structure of this distribution. However, according to first-order direct reaction theory it can be shown that the ratio of the cross section of the first excited state to that of the second is given by

$$\frac{d\sigma(\rightarrow 9/2^-)}{d\sigma(\rightarrow 11/2^-)}=\left[\frac{(\frac{7}{2},\frac{7}{2},2,0|\frac{9}{2},\frac{7}{2})}{(\frac{7}{2},\frac{7}{2},2,0|11/2,\frac{7}{2})}\right]^2=35/9. \quad (1)$$

This ratio assumes only that the first two levels are members of the ground state $K=\frac{7}{2}$ rotational band and is independent of the distortion. It is clear from the data that the observed ratio is more nearly 2. The difference between the observed and predicted ratio may be due to another unresolved level enhancing the cross section of the second excited state which is generally acknowledged

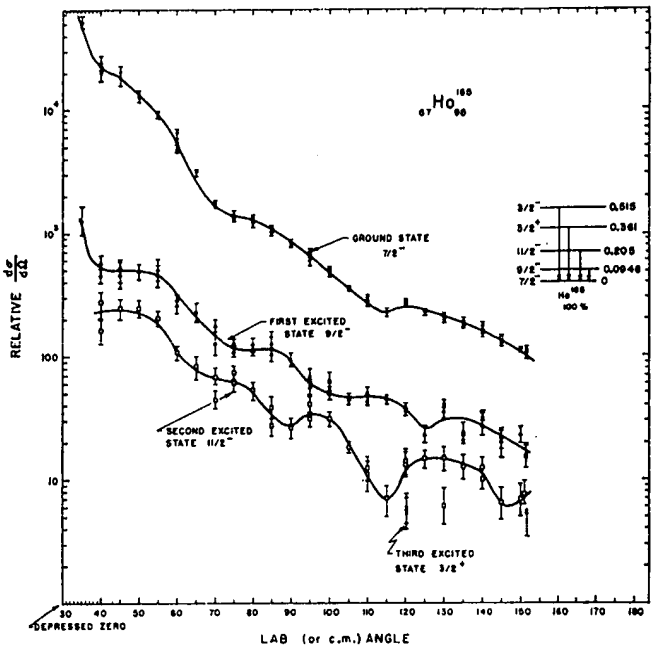

FIG. 5. Angular distributions for the ground state and first two excited states of holmium 165.

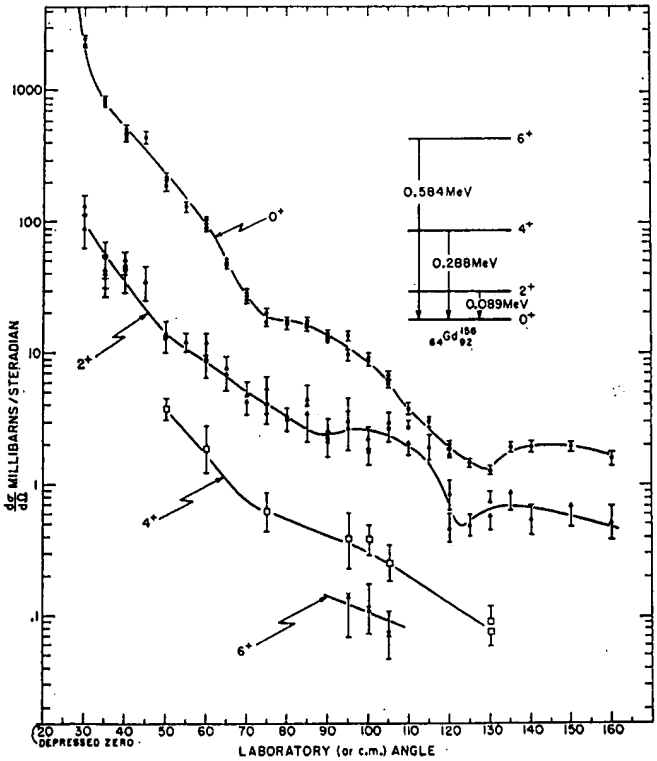

FIG. 6. Angular distributions for the ground state and first two excited states of gadolinium 156.

to be 205 keV.[22] This unresolved level might be that reported to be at 277 keV by Hashizume *et al.*[23]

B. Gadolinium-156

A spectrum for Gd^{156} is shown in Fig. 4. In this and other runs there is evidence that the 6^+ level is weakly excited by 17.5-MeV incident protons. Angular distributions for the ground state and first two excited states are shown in Fig. 6. The error bars reflect statistical uncertainties as well as errors in peak separation. In each run the elastic oxygen peak and the elastic carbon peaks were displayed and used as a cross-section check. The angular distributions taken for oxygen elastics agreed within 5% with those taken previously in this laboratory.[19] The amount of oxygen in the target was accurately known from the composition of the oxide Gd_2O_3. It is felt that the error in determination of the gadolinium ground-state cross sections is less than 10%.

[22] F. Ajzenberg-Selove, N. B. Gove, T. Lauritsen, C. L. McGinnis, R. Nakasima, J. Scheer, and K. Way, in *Energy Levels of Nuclei: A = 5 to A = 257* (Springer-Verlag, Berlin, 1961).
[23] A. Hashizume, T. Takahashi, Y. Tend, and Y. Enomota, J. Phys. Soc. Japan 15, 2175 (1960).

ACKNOWLEDGMENTS

The authors wish to thank Dr. John Blair for suggesting the problem and for his useful comments as the investigation unfolded. We are indebted to Dr. R. Sherr for his aid in solving vexing experimental problems, to Dr. E. Rost for his theoretical discussions and aid in the preparation of this paper, and to Dr. W. W. Daehnick for allowing us to use his oxygen data prior to publication.

PHYSICAL REVIEW VOLUME 132, NUMBER 6 15 DECEMBER 1963

Disintegration of the Deuteron in a Coulomb Field

RAYMOND GOLD
Argonne National Laboratory, Argonne, Illinois
AND
CALVIN WONG
Lawrence Radiation Laboratory, University of California, Livermore, California
(Received 7 August 1963)

The Coulomb disintegration of the deuteron is treated by means of perturbation theory. The breakup cross section is determined in the electric-dipole approximation. Total cross sections have been calculated for deuteron laboratory energies below 25 MeV and for target nuclei in the range $4 \leq Z \leq 92$. The results of these calculations are compared with earlier theoretical estimates and recent experimental measurements.

INTRODUCTION

In low-energy deuteron reactions there may exist processes which compete favorably with direct nuclear stripping. A complete analysis of such reactions may then comprise contributions due to electric breakup, nuclear disintegration, and evaporation from compound nucleus formation. The electric breakup aspects of this problem have been considered by Dancoff[1] for 200-MeV deuterons, by Mullin and Guth[2] for 15-MeV deuterons, and for lower energy deuterons by Landau and Lifshitz.[3] A critical review of much of this work has been given by Breit.[4] Disintegration due to nuclear potential as well as Coulomb disintegration has been theoretically investigated by Akhieser and Sitenko.[5]

More recently, Hamburger *et al.*[6] have adopted a semiclassical breakup model to fit experimental results obtained with 15-MeV deuterons. However, due to an error,[7] the calculated values of the angle of maximum intensity are incorrect. It now appears that the simple semiclassical model of deuteron breakup does not satisfactorily account for the observed angle of maximum intensity of the continuum protons. An integral of this continuum for[6] $E_p \leq E_D - 2.2$ MeV yields total cross sections much larger than that calculated for either electric[2] or nuclear[5] breakup. This implies a serious disagreement with theoretical estimates assuming negligible contributions from compound nucleus and direct stripping processes.

Recently, Anderson and Bauer[8] have attempted to

[1] S. Dancoff, Phys. Rev. 72, 1017 (1947).
[2] C. Mullin and E. Guth, Phys. Rev. 82, 141 (1951).
[3] L. D. Landau and E. M. Lifshitz, Zh. Eksperim. i Teor. Fiz. 18, 750 (1948).
[4] G. Breit, in *Handbuch der Physik*, edited by S. Flügge (Springer-Verlag, Berlin, 1959), Vol. 41, Sec. 1, pp. 304–320.
[5] A. Akhieser and A. Sitenko, Phys. Rev. 106, 1236 (1957).
[6] E. Hamburger, B. Cohen, and R. Price, Phys. Rev. 121, 1143 (1961).
[7] If $\theta = \theta_p + \theta_d$, where θ is the angle of deflection, then Eq. (3) of Ref. 6 should read
$$q = (Ze^2/2E_p)(1+\csc\theta_p) = (Ze^2/2E_d)(1+\csc\theta_d).$$
[8] J. D. Anderson and R. Bauer (private communication).